Thermodynamically consistent plastic-damage framework for localized failure in quasi-brittle solids: material model and strain localization analysis

Jian-Ying Wu*

State Key Laboratory of Subtropical Building Science, South China University of Technology, 510641 Guangzhou, China.

Miguel Cervera

CIMNE, Technical University of Catalonia, Edificio C1, Campus Norte, Jordi Girona 1-3, 08034 Barcelona, Spain.

Abstract

Aiming for the modeling of localized failure in quasi-brittle solids, this paper addresses a thermodynamically consistent plastic-damage framework and the corresponding strain localization analysis. A unified elastoplastic damage model is first presented based on two alternative kinematic decompositions, with the evolution laws of involved internal variables characterized by a dissipative flow tensor. For the strong (or the equivalent regularized) discontinuity to form in such an inelastic quasi-brittle solids and to evolve eventually into a fully softened one, a novel strain localization analysis is then suggested. A kinematic constraint more demanding than the classical discontinuous bifurcation condition is derived by accounting for the traction continuity and the loading/unloading deformation states compatible with the strong (or regularized) discontinuity. More specifically, the strain jumps characterized by Maxwell's kinematic condition have to be completely inelastic (energy dissipative). Reproduction of the above kinematics implies vanishing of the aforesaid dissipative flow tensorial components in the directions orthogonal to the discontinuity orientation. This property naturally allows developing a localized plastic-damage model for the discontinuity (band), with its orientation and the traction-based failure criterion consistently determined *a posteriori* from the given stress-based counterpart. The general results are then particularized to the 2D conditions of plane stress and plane strain. It is found that in the case of plane stress, strain localization into a strong (or regularized) discontinuity can occur at the onset of strain softening. Contrariwise, owing to an extra kinematic constraint, in the condition of plane strain some continuous inelastic deformations and substantial re-orientation of principal strain directions in general have to take place in the softening regime prior to strain localization. The classical Rankine, Mohr-Coulomb, von Mises (J_2) and Drucker-Prager criteria are finally analyzed as illustrative examples. In particular, the closed-form discontinuity angles coincident with numerical simulations and the corresponding traction-based failure criteria are obtained.

Keywords:

Localized failure; damage; plasticity; fracture; constitutive behavior; strain localization; concrete.

*Tel.: (+86) 20-87112787

Email address: jywu@scut.edu.cn (Jian-Ying Wu)

1. Introduction

The onset of macroscopic failure in solids and structures is often signified by highly localized deformations (i.e., strain localization) within bands of small (or even fracture surfaces of negligible) width compared to the length scale of the structure in consideration. Typical examples of the above strain localization manifestation include cracks in concrete, joints in rocks, shear bands in soils, dislocations and slip lines in metals, etc., owing to the overall softening responses of these solids. It is of utmost significance to resolve strain localization and the resulting localized failure while evaluating the structure performances and preventing the potential catastrophic collapse.

Ever since the pioneering work of Ngo and Scordelis [38] and Rashid [48] a large number of different approaches have been developed for the modeling of localized failure in quasi-brittle solids. These approaches range from the classical discrete and smeared crack models [51], to the more advanced strong discontinuity approaches [22, 39, 56, 61, 70, 71]. Restricting the focus to the continuum context, existing formulations can be classified into stress-based (generalized) continuum models or traction-based nonlinear fracture models. In the stress-based continuum model the strain/displacement discontinuities upon strain localization are smoothed or smeared. Accordingly, the overall nonlinear behavior of the weakened solid can be described by a tensorial constitutive law in terms of stress vs. strain equipped with internal variables. Plasticity [13, 14] and damage mechanics [32] or their combination [3, 59, 69] are frequently employed to develop appropriate inelastic constitutive laws; see Abu Al-Rub and Darabi [1] and the references therein. To guarantee objectivity of the energy dissipation during the failure process, the softening regime is generally regularized by introducing the fracture energy and an appropriately identified length scale [7]. Comparatively, in the traction-based approach strain/displacement jumps are explicitly accounted for by embedding the discontinuities into a solid matrix along preferred orientations. It is in general assumed that energy dissipation is localized into the discontinuities while the bulk remains elastic, between which the traction continuity condition is imposed. Depending on the recoverable/irreversible properties of the discontinuities, vectorial traction-based cohesive zone models of either plastic [8], damage [2, 30] or combined plastic-damage [62, 67] type can be established. Similarly, the softening law for the discontinuities is also characterized by the fracture energy.

In the traction-based modeling of localized failure in solids, a crucial step is to determine the discontinuity orientation consistently and fix it appropriately, if required. This is a non-trivial task for a new or propagating discontinuity whose orientation is not pre-defined or known *a priori*. For strain or weak discontinuities, the discontinuous bifurcation analysis, pioneered by Hill [23, 24], Thomas [57] and Rice [50, 52], nowadays becomes the standard tool. Based on the assumption of linear comparison solid (inelastic loading state in both the bulk and localization band) and the traction continuity condition, necessary conditions for discontinuous bifurcation were identified and formulations for the orientation of shear bands were obtained for plastic materials; see the monograph [33] and the articles [31, 53, 55, 58, 60] among many others. Franz et al. [18, 19] analyzed the limit to ductility of steel with the Rice bifurcation criterion and a self consistent visco-plastic model. Recently, Sánchez et al. [54] and Huespe et al. [27, 28] successfully applied this strategy to the modeling of ductile fracture in which the stress triaxility is important [6, 49].

Dequiedt [17] developed a variational approach to catch localization of deformation in the microstructure of heterogeneous materials and applied it to polycrystalline solids.

For strong discontinuities in quasi-brittle solids, similar arguments were also followed. For instance, Simó et al. [56] and Oliver [39] suggested using the discontinuous bifurcation condition together with *null* softening modulus to determine the discontinuity orientation. However, its application to strong discontinuities in quasi-brittle solids might be questionable, since the actual deformation states upon strain localization, i.e., inelastic loading inside the discontinuity (band) and unloading elastically outside it, are inconsistent with the assumption of linear comparison solids. Consequently, except for some particular cases (e.g., the Rankine and plane strain von Mises models), the strong discontinuity condition [40–42] cannot be satisfied in general cases [41]. Some kinematics mismatches are observed [45, 46] due to mis-prediction of the discontinuity orientation, inevitably resulting in stress locking [10, 36]. This fact partially explains the overwhelming popularity of the maximum tensile stress criterion or linear fracture mechanics based ones [16] in the modeling of localized failure in brittle and quasi-brittle solids [70, 71].

Provided the discontinuity orientation is determined, a cohesive zone model is generally introduced to characterize the discontinuities, resulting in either the strong/regularized or embedded/smeared discontinuity models; see Cervera and Wu [12] for the conformity between these traction-based approaches. However, on the one hand, it is difficult to identify the traction-based failure criterion and involved model parameters from available experimental data. On the other hand, the questions whether and when the traction-based cohesive zone model should be introduced cannot be easily answered. Therefore, it would be rather advantageous, if the traction-based failure criterion is derived consistently from a stress-based one and the right instant for introducing the cohesive zone model can be also identified. In this aspect, Oliver and coworkers [40–43, 45] made great contributions and derived cohesive zone models by projecting inelastic material laws onto the discontinuity orientation. However, only the classical isotropic damage model [42, 43, 45], the Rankine and plane strain von Mises plasticity models [40, 41] are considered, whereas more general material constitutive laws cannot been sufficiently accounted for [41]: "*Obtaining such explicit forms of the discrete constitutive equations is not so straight-forward for other families of elastoplastic models*".

Noticing the above facts, Cervera et al. [10] proposed directly using the strong discontinuity condition [40–42] to determine the discontinuity orientation, so that the stress locking-free property can be guaranteed for a fully softened discontinuity. The obtained discontinuity angles for von Mises (J_2) plasticity model were validated by numerical simulations in the cases of plane stress and plane strain. Recently, the authors [63–66] successfully extended this method to a stress-based plastic-damage model with general failure criterion. Not only the discontinuity orientation but also the traction-based failure criterion are determined consistently from the given stress-based counterpart. Furthermore, the bi-directional connections and in particular the equivalence conditions between two complementary methodologies for the modeling of localized failure in quasi-brittle solids, i.e., *traction-based discontinuities localized in an elastic solid and strain localization of a stress-based inelastic softening solid*, have also been established. However, all our previous work implicitly or explicitly assumes that upon strain localization, *only relative rigid body motions* occur at both sides of the discontinuity (band). This restrictive kinematics implies continuous bulk strains across the

discontinuity [62]. Though the discontinuous bulk strains seldom dominates strain localization in quasi-brittle solids [44, 70], the resulting stress continuity might be too restrictive in some cases. Moreover, the aforementioned analyses were mainly intended for the plane stress condition, and the exceptional cases which preclude occurrence of a strong (or the equivalent regularized) discontinuity were not considered.

The aim of this paper is to make further contributions to the above topics. The novelties are threefold: *(i)* The Maxwell's kinematic condition for guaranteeing the occurrence of a strong discontinuity is derived from the traction continuity condition together with the consistent loading/unloading deformation states upon strain localization in quasi-brittle solids; in particular, the assumption of continuous stresses across the discontinuity is disregarded; *(ii)* Closed-form results in both plane stress and plane strain conditions, coincident with those given by numerical simulations [11], are obtained, and the consequences of an additional out-of-plane constraint in the later case are identified; *(iii)* The aforesaid exceptional case in which the strong discontinuity is precluded for a given stress-based failure criterion is solved by introducing necessary modifications based on the equivalence between traction- and stress-based approaches established before [66].

This paper is organized as follows. After this introduction, a unified elastoplastic damage framework is presented in Section 2 based on the irreversible thermodynamics with internal variables. Section 3 addresses the Maxwell's kinematic constraint upon strain localization in quasi-brittle solids and its application to the above elastoplastic damage model. Closed-form results in 2D conditions of plane stress and plane strain are given in Section 4, together with several classical failure criteria analyzed as illustrative examples. The most relevant conclusions are drawn in Section 5. For the sake of completeness, two appendices are attached to close this paper.

Notation. Compact tensor notation is used in this paper as far as possible. As a general rule, scalars are denoted by italic light-face Greek or Latin letters (e.g. a or λ); vectors and second-order tensors are signified by italic boldface minuscule and majuscule letters like $\boldsymbol{a}$ and $\boldsymbol{A}$, respectively. Fourth-order tensors are identified by blackboard-bold majuscule characters (e.g. $\mathbb{A}$). Symbols $\boldsymbol{I}$ and $\mathbb{I}$ represent the second-order and symmetric fourth-order identity tensors, respectively. Superscripts '$^{\mathrm{T}}$' and '$^{\mathrm{sym}}$' indicate the transposition and symmetrization operations, respectively. The inner products with single and double contractions are denoted by '$\cdot$' and ':', respectively. The dyadic product '$\otimes$' and the symmetrized Kronecker product $\overline{\otimes}$ are defined as

$$\left(\boldsymbol{A}\otimes\boldsymbol{B}\right)_{ijkl}=A_{ij}B_{kl},\qquad \left(\boldsymbol{A}\,\overline{\otimes}\,\boldsymbol{B}\right)_{ijkl}=\frac{1}{2}\left(A_{ik}B_{jl}+A_{il}B_{jk}\right)$$

2. A unified elastoplastic damage framework

In this section a unified elastoplastic damage framework [34, 67] is presented. It is based on the irreversible thermodynamics with internal variables [26]. Both stress- and traction-based elastoplastic damage models can be developed within this framework.

2.1. Stress–strain relations

Confining the discussion to a purely mechanical theory, the second law of thermodynamics (local form) requires that for any admissible deformation process, the energy dissipation $\mathscr{D}$ has to be non-negative, i.e.,

$$\mathscr{D} := \boldsymbol{\sigma} : \dot{\boldsymbol{\epsilon}} - \dot{\psi} \geq 0 \tag{2.1}$$

where $\boldsymbol{\sigma}$ and $\boldsymbol{\epsilon}$ denote the second-order stress and strain tensors, respectively; ψ is the free energy density function of the material; $\dot{()}$ represents the rate with respect to the (pseudo-) time.

To account for both stiffness degradation and irreversible deformations, the free energy density function ψ is postulated as

$$\psi = \psi^{\mathrm{ed}}(\boldsymbol{\epsilon} - \boldsymbol{\epsilon}^{\mathrm{p}}, \mathbb{E}) + \chi(\kappa) \tag{2.2}$$

For a linear hyperelastic material, the stored strain energy density function $\psi^{\mathrm{ed}}(\cdot,\cdot)$ is expressed as a quadratic form in terms of the recoverable (elastic and damage) strain tensor $\boldsymbol{\epsilon} - \boldsymbol{\epsilon}^{\mathrm{p}}$ and the (variable) fourth-order material (unloading) stiffness tensor $\mathbb{E}$, i.e.,

$$\psi^{\mathrm{ed}} = \frac{1}{2}\left(\boldsymbol{\epsilon} - \boldsymbol{\epsilon}^{\mathrm{p}}\right) : \mathbb{E} : \left(\boldsymbol{\epsilon} - \boldsymbol{\epsilon}^{\mathrm{p}}\right) \tag{2.3}$$

with $\boldsymbol{\epsilon}^{\mathrm{p}}$ being the irreversible plastic strain tensor. Furthermore, the inelastic potential function $\chi(\cdot)$ is characterized by a single *strain-like* internal variable κ. Note that the stiffness tensor $\mathbb{E}$ (or, equivalently, the compliance $\mathbb{C} = \mathbb{E}^{-1}$), the plastic strain tensor $\boldsymbol{\epsilon}^{\mathrm{p}}$ and the strain-like variable κ are all internal variables. Therefore, their evolution laws have to be postulated.

Making use of standard arguments yields the following constitutive relations

$$\boldsymbol{\sigma} = \frac{\partial \psi^{\mathrm{ed}}}{\partial\left(\boldsymbol{\epsilon} - \boldsymbol{\epsilon}^{\mathrm{p}}\right)} = \mathbb{E} : \left(\boldsymbol{\epsilon} - \boldsymbol{\epsilon}^{\mathrm{p}}\right), \qquad \boldsymbol{\epsilon} = \mathbb{C} : \boldsymbol{\sigma} + \boldsymbol{\epsilon}^{\mathrm{p}} \tag{2.4}$$

or the rate form

$$\dot{\boldsymbol{\sigma}} = \mathbb{E} : \left(\dot{\boldsymbol{\epsilon}} - \dot{\boldsymbol{\epsilon}}^{\mathrm{dis}}\right), \qquad \dot{\boldsymbol{\epsilon}} = \mathbb{C} : \dot{\boldsymbol{\sigma}} + \dot{\boldsymbol{\epsilon}}^{\mathrm{dis}} \tag{2.5}$$

where the *dissipative strain tensor rate* $\dot{\boldsymbol{\epsilon}}^{\mathrm{dis}}$ is defined as

$$\dot{\boldsymbol{\epsilon}}^{\mathrm{dis}} := \dot{\mathbb{C}} : \boldsymbol{\sigma} + \dot{\boldsymbol{\epsilon}}^{\mathrm{p}} \tag{2.6}$$

with $\dot{\mathbb{C}} : \boldsymbol{\sigma}$ and $\dot{\boldsymbol{\epsilon}}^{\mathrm{p}}$ being its damage and plastic components, respectively; see Fig. 1. Note that the dissipative strain tensor rate $\dot{\boldsymbol{\epsilon}}^{\mathrm{dis}}$ does not correspond to an actual "strain"; it is only defined in rate form when the involved energy dissipative mechanisms, i.e., damage evolution and plastic flows, are active.

As shown in Fig. 2, the strain tensor $\boldsymbol{\epsilon}$ and the rate $\dot{\boldsymbol{\epsilon}}$ can also be rewritten as the kinematic decomposition adopted in the classical smeared crack model [3, 51]

$$\boldsymbol{\epsilon} = \boldsymbol{\epsilon}^{\mathrm{e}} + \boldsymbol{\epsilon}^{\mathrm{in}} = \mathbb{C}^{\mathbf{0}} : \boldsymbol{\sigma} + \boldsymbol{\epsilon}^{\mathrm{in}}, \qquad \dot{\boldsymbol{\epsilon}} = \dot{\boldsymbol{\epsilon}}^{\mathrm{e}} + \dot{\boldsymbol{\epsilon}}^{\mathrm{in}} = \mathbb{C}^{\mathbf{0}} : \dot{\boldsymbol{\sigma}} + \dot{\boldsymbol{\epsilon}}^{\mathrm{in}} \tag{2.7}$$

Accordingly, the stress $\boldsymbol{\sigma}$ and the rate $\dot{\boldsymbol{\sigma}}$ are given by

$$\boldsymbol{\sigma} = \mathbb{E}^0 : \boldsymbol{\epsilon}^{\mathrm{e}} = \mathbb{E}^0 : \left(\boldsymbol{\epsilon} - \boldsymbol{\epsilon}^{\mathrm{in}}\right), \qquad \dot{\boldsymbol{\sigma}} = \mathbb{E}^0 : \dot{\boldsymbol{\epsilon}}^{\mathrm{e}} = \mathbb{E}^0 : \left(\dot{\boldsymbol{\epsilon}} - \dot{\boldsymbol{\epsilon}}^{\mathrm{in}}\right) \tag{2.8}$$

with $\mathbb{E}^0$ and $\mathbb{C}^0$ being the elastic stiffness and compliance of the material, respectively. In the above constitutive relations, the elastic and inelastic strain tensors $(\boldsymbol{\epsilon}^{\mathrm{e}}, \boldsymbol{\epsilon}^{\mathrm{in}})$ are given by

$$\epsilon^{\mathrm{e}} = \mathbb{C}^0 : \boldsymbol{\sigma}, \qquad \boldsymbol{\epsilon}^{\mathrm{in}} = \boldsymbol{\epsilon}^{\mathrm{d}} + \boldsymbol{\epsilon}^{\mathrm{p}} = \mathbb{C}^{\mathrm{d}} : \boldsymbol{\sigma} + \boldsymbol{\epsilon}^{\mathrm{p}} \tag{2.9}$$

where the damage strain tensor $\epsilon^{\mathrm{d}} := \mathbb{C}^{\mathrm{d}} : \boldsymbol{\sigma}$ represents the *recoverable* inelastic strain; the fourth-order damage compliance $\mathbb{C}^{\mathrm{d}}$ is defined as $\mathbb{C}^{\mathrm{d}} := \mathbb{C} - \mathbb{C}^0$, with identical evolution law $\dot{\mathbb{C}}^{\mathrm{d}} = \dot{\mathbb{C}}$.

Remark 2.1 Similarly to the kinematic decomposition (2.7), the stored strain energy density (equal in magnitude to the complementary energy density for a linear hyperelastic material) ψ^{ed} defined in Eq. (2.3) can be decomposed as

$$\psi^{\mathrm{ed}} = \frac{1}{2}\,\boldsymbol{\sigma} : \mathbb{C} : \boldsymbol{\sigma} = \psi^{\mathrm{e}} + \psi^{\mathrm{d}} \tag{2.10}$$

where the elastic and damage strain energy densities (also equal in magnitude to their complementary counterparts) $(\psi^{\mathrm{e}}, \psi^{\mathrm{d}})$ are given by

$$\psi^{\mathrm{e}} = \frac{1}{2}\,\boldsymbol{\sigma} : \mathbb{C}^0 : \boldsymbol{\sigma} = \frac{1}{2}\,\boldsymbol{\sigma} : \boldsymbol{\epsilon}^{\mathrm{e}} = \frac{1}{2}\,\boldsymbol{\epsilon}^{\mathrm{e}} : \mathbb{E}^0 : \boldsymbol{\epsilon}^{\mathrm{e}} \tag{2.11a}$$

$$\psi^{\mathrm{d}} = \frac{1}{2}\,\boldsymbol{\sigma} : \mathbb{C}^{\mathrm{d}} : \boldsymbol{\sigma} = \frac{1}{2}\,\boldsymbol{\sigma} : \boldsymbol{\epsilon}^{\mathrm{d}} = \frac{1}{2}\,\boldsymbol{\epsilon}^{\mathrm{e}} : \mathbb{E}^0 : \boldsymbol{\epsilon}^{\mathrm{d}} \tag{2.11b}$$

Note again the recoverable nature of the damage strain $\boldsymbol{\epsilon}^{\mathrm{d}}$ and the corresponding energy density ψ^{d} upon unloading. ■

2.2. Evolution laws and rate constitutive relations

Besides the above constitutive relations, the following energy dissipation inequality has to be satisfied

$$\mathscr{D} = \frac{1}{2}\,\boldsymbol{\sigma} : \dot{\mathbb{C}} : \boldsymbol{\sigma} + \boldsymbol{\sigma} : \dot{\boldsymbol{\epsilon}}^{\mathrm{p}} - \dot{\chi} = \frac{1}{2}\,\boldsymbol{\sigma} : \dot{\mathbb{C}} : \boldsymbol{\sigma} + \boldsymbol{\sigma} : \dot{\boldsymbol{\epsilon}}^{\mathrm{p}} + \left(q^0 - q\right) \cdot \dot{\kappa} \geq 0 \tag{2.12}$$

where $q^0 - q := -\partial\chi/\partial\kappa$ denotes the stress-like internal variable conjugate to the strain-like one κ, with q^0 being the initial value of the residual material strength $q(\kappa)$, i.e., $q^0 := q(\kappa = 0)$.

Let us consider a rate-independent inelastic softening solid characterized by the failure criterion $\mathcal{F}(\boldsymbol{\sigma}, q) \leq 0$, where the loading function $\mathcal{F}(\boldsymbol{\sigma}, q)$ is a convex, smooth and differentiable homogeneous function of degree $M \geq 1$, i.e.,

$$\mathcal{F}(\boldsymbol{\sigma}, q) = \frac{1}{M}\left(\partial_{\boldsymbol{\sigma}}\mathcal{F} : \boldsymbol{\sigma} + \partial_q\mathcal{F} \cdot q\right) = \frac{1}{M}\left(\boldsymbol{\Lambda} : \boldsymbol{\sigma} - h \cdot q\right) \tag{2.13}$$

for the derivatives $\boldsymbol{\Lambda} := \partial\mathcal{F}/\partial\boldsymbol{\sigma}$ and $h := -\partial\mathcal{F}/\partial q$. As will be shown, either stress- or traction-based loading function $\mathcal{F}(\boldsymbol{\sigma}, q)$ can be employed in the modeling of localized failure in solids.

Accordingly, the postulate of maximum energy dissipation gives the following associated evolution laws [34, 67]

$$\dot{\boldsymbol{\epsilon}}^{\mathrm{dis}} = \dot{\mathbb{C}} : \boldsymbol{\sigma} + \dot{\boldsymbol{\epsilon}}^{\mathrm{p}} = \lambda \boldsymbol{\Lambda}, \qquad \dot{\kappa} = \lambda h \tag{2.14}$$

where the *dissipative flow tensor* $\boldsymbol{\Lambda} := \partial \mathcal{F} / \partial \boldsymbol{\sigma}$ is normal to the failure surface $\mathcal{F}(\boldsymbol{\sigma}, q) = 0$; the Lagrangian multiplier λ satisfies the classical Kuhn-Tucker loading/unloading conditions

$$\lambda \geq 0, \qquad \mathcal{F}(\boldsymbol{\sigma}, q) \leq 0, \qquad \lambda \mathcal{F}(\boldsymbol{\sigma}, q) = 0 \tag{2.15}$$

Note that the convex loading function (2.13) and the associated evolution laws (2.14) automatically guarantees the energy dissipation inequality (2.12) for any softening law $q(\kappa)$; see Wu and Cervera [65].

To differentiate the damage and plastic contributions to the dissipative strain tensor rate $\dot{\boldsymbol{\epsilon}}^{\mathrm{dis}}$, a material parameter $\xi \in [0, 1]$ is introduced so that [34, 47, 67]

$$\dot{\boldsymbol{\epsilon}}^{\mathrm{p}} = \big(1 - \xi\big)\, \dot{\boldsymbol{\epsilon}}^{\mathrm{dis}} = \big(1 - \xi\big)\, \lambda \boldsymbol{\Lambda} \tag{2.16a}$$

$$\dot{\mathbb{C}} : \boldsymbol{\sigma} = \xi\, \dot{\boldsymbol{\epsilon}}^{\mathrm{dis}} = \xi\, \lambda \boldsymbol{\Lambda} \tag{2.16b}$$

For the homogeneous loading function (2.13), the evolution law for the compliance $\mathbb{C}$ satisfying Eq. (2.16b) is given by [34, 67]

$$\dot{\mathbb{C}} = \dot{\mathbb{C}}^{\mathrm{d}} = \xi\, \lambda \frac{\boldsymbol{\Lambda} \otimes \boldsymbol{\Lambda}}{\boldsymbol{\Lambda} : \boldsymbol{\sigma}} \tag{2.17}$$

as long as the condition $\boldsymbol{\Lambda} : \boldsymbol{\sigma} \neq 0$ is satisfied. The cases $\xi = 0$ and $\xi = 1$ correspond to the classical plasticity model [14] and the elastic damage (degradation) model [9, 68], respectively. For the parameter $\xi \in (0, 1)$, both the material compliance $\mathbb{C}$ (or the damage one $\mathbb{C}^{\mathrm{d}}$) and the plastic strain $\boldsymbol{\epsilon}^{\mathrm{p}}$ are internal variables, resulting in a combined plastic-damage model.

When the material is unloading, i.e., $\mathcal{F}(\boldsymbol{\sigma}, q) < 0$, it follows that $\lambda = 0$; for the loading case, $\lambda > 0$ is solved from the consistency condition $\dot{\mathcal{F}}(\boldsymbol{\sigma}, q) = 0$ as

$$\lambda = \frac{\boldsymbol{\Lambda} : \mathbb{E} : \dot{\boldsymbol{\epsilon}}}{\boldsymbol{\Lambda} : \mathbb{E} : \boldsymbol{\Lambda} + h \cdot H \cdot h} = \frac{\boldsymbol{\Lambda} : \dot{\boldsymbol{\sigma}}}{h \cdot H \cdot h} \tag{2.18}$$

for the softening modulus $H := \partial q / \partial \kappa < 0$. Therefore, the rate constitutive relations are given by

$$\dot{\boldsymbol{\sigma}} = \mathbb{E}_{\mathrm{tan}} : \dot{\boldsymbol{\epsilon}}, \qquad \dot{\boldsymbol{\epsilon}} = \mathbb{C}_{\mathrm{tan}} : \dot{\boldsymbol{\sigma}} \tag{2.19}$$

where the material tangents $\mathbb{E}_{\mathrm{tan}}$ and $\mathbb{C}_{\mathrm{tan}}$ for the loading state (i.e., $\lambda > 0$) are expressed as

$$\mathbb{E}_{\mathrm{tan}} = \mathbb{E} - \frac{\mathbb{E} : \big(\boldsymbol{\Lambda} \otimes \boldsymbol{\Lambda}\big) : \mathbb{E}}{\boldsymbol{\Lambda} : \mathbb{E} : \boldsymbol{\Lambda} + h \cdot H \cdot h} \tag{2.20a}$$

$$\mathbb{C}_{\mathrm{tan}} = \mathbb{C} + \frac{\boldsymbol{\Lambda} \otimes \boldsymbol{\Lambda}}{h \cdot H \cdot h} \tag{2.20b}$$

both being symmetric due to the associated evolution laws considered.

2.3. Fracture energy

For the above plastic-damage model the external energy density supplied to the solid during the failure process, or the so-called specific fracture energy (i.e., energy dissipation per unit volume) g_{f}, can be evaluated as [65, 66]

$$g_{\mathrm{f}} = \int_0^\infty \boldsymbol{\sigma} : \mathrm{d}\boldsymbol{\epsilon} = \left(1 - \frac{1}{2}\xi\right) \int_0^\infty q(\kappa)\, \mathrm{d}\kappa = \frac{G_{\mathrm{f}}}{b} \tag{2.21}$$

where G_{f} is the fracture energy (i.e., energy dissipation per unit surface area), assumed as a material property; b is a regularization width (see the discussion in next section) where the energy dissipation localizes. Therefore, the softening law $q(\kappa)$ has to be regularized with respect to the localized band width b in such a way that the energy dissipation during the whole failure process does not depend on it.

The above regularized procedure was advocated in the crack band theory [7]. It is equivalent to the cohesive (fictitious) crack model [5, 15, 25]. In this latter context, Eq. (2.21) is rewritten as

$$G_{\mathrm{f}} = b g_{\mathrm{f}} = \left(1 - \frac{1}{2}\xi\right) \int_0^\infty q(\kappa) b\, \mathrm{d}\kappa = \left(1 - \frac{1}{2}\xi\right) \int_0^\infty q(\tilde{\kappa})\, \mathrm{d}\tilde{\kappa} \tag{2.22}$$

It then allows introducing an equivalent softening law $q(\tilde{\kappa})$ expressed in terms of the alternative *displacement-like* internal variable $\tilde{\kappa}$

$$\tilde{\kappa} := b\kappa, \qquad \dot{\tilde{\kappa}} = \tilde{\lambda} h \qquad \Longrightarrow \qquad \widetilde{H} = \frac{1}{b} H, \qquad \lambda = \frac{1}{b}\tilde{\lambda} \tag{2.23}$$

for the displacement-driven softening modulus $\widetilde{H} := \partial q / \partial \tilde{\kappa}$ and the corresponding Lagrangian multiplier $\tilde{\lambda} \geq 0$.

Remark 2.2 It is concluded from Eqs. (2.23) that the kinematic internal variables characterizing the inelastic behavior of the material, e.g., the damage compliance $\mathbb{C}^{\mathrm{d}}$, the plastic strain $\boldsymbol{\epsilon}^{\mathrm{p}}$ and the inelastic strain $\boldsymbol{\epsilon}^{\mathrm{in}}$, etc., are all inversely proportional to the band width b. ■

3. Strain localization analysis

In this section, strain localization in an inelastic solid characterized by the above elastoplastic damage model is analyzed. Compared to the classical discontinuous bifurcation analysis [23, 24, 50, 52, 53, 57], the traction continuity and stress boundedness are guaranteed [10, 63, 64] by reproducing the Maxwell's discontinuity kinematics. More specifically, upon strain localization the dissipative flow tensor characterizing the inelastic evolution laws evolves into a particular structure in terms of an dissipative flow vector and the discontinuity orientation. Accordingly, the tensorial flow components in the directions orthogonal to the discontinuity orientation have to vanish so that the consistent loading/unloading stress states upon strain localization are correctly represented and a fully stress-free discontinuity (band) can eventually form. This property allows developing a traction-based plastic-damage model for the discontinuity (band). Both the discontinuity orientation and the traction-based failure criterion can be determined *a posterior* from the given stress-based counterpart.

3.1. Discontinuity kinematics

Let us consider the domain $\Omega \subset \mathbb{R}^{n_{\text{dim}}}$ ($n_{\text{dim}} = 1, 2, 3$) shown in Fig. 3. It is occupied by a solid with reference position vector $\boldsymbol{x} \in \mathbb{R}^{n_{\text{dim}}}$. The boundary is denoted by $\Gamma \subset \mathbb{R}^{n_{\text{dim}}-1}$, with an external unit normal vector $\boldsymbol{n}^*$. Deformations of the solid are characterized by the displacement field $\boldsymbol{u} : \Omega \to \mathbb{R}^{n_{\text{dim}}}$ and the infinitesimal strain field $\boldsymbol{\epsilon} := \nabla^{\text{sym}}\boldsymbol{u}$, with $\nabla(\cdot)$ being the spatial gradient operator. The solid is subjected to a distributed body force $\boldsymbol{b}^* : \Omega \to \mathbb{R}^{n_{\text{dim}}}$ per unit volume. Surface tractions $\boldsymbol{t}^* : \Gamma_t \to \mathbb{R}^{n_{\text{dim}}}$ and displacements $\boldsymbol{u}^* : \Gamma_u \to \mathbb{R}^{n_{\text{dim}}}$ are imposed on the disjoint and complementary parts $\Gamma_t \subset \Gamma$ and $\Gamma_u \subset \Gamma$ of the boundary Γ, respectively.

At the early stage of the deformation process, standard compatibility relations of a continuum medium apply. That is, both the displacement and strain fields are continuous and regular (bounded). Upon satisfaction of a specific criterion, strain localization occurs, inevitably inducing strain/displacement jumps. To approximate these jumps, a strong (or a regularized) discontinuity may be introduced. In either case, the standard kinematics no longer applies.

Displacement jumps can be described by a strong discontinuity. As depicted in Fig. 4(a), the strong discontinuity $\mathcal{S}$ splits the solid Ω into two parts Ω^+ and Ω^-, located "ahead of" and "behind" $\mathcal{S}$, respectively, in such a way that $\Omega^+ \cup \Omega^- \cup \mathcal{S} = \Omega$. The discontinuity orientation is characterized by a unit normal vector $\boldsymbol{n}$, pointing from Ω^- to Ω^+ and fixed along time (i.e., $\dot{\boldsymbol{n}} = \boldsymbol{0}$). The strong discontinuity $\mathcal{S}$ causes displacement jumps $\boldsymbol{w} := \boldsymbol{u}(\boldsymbol{x} \in \Omega^+ \cap \mathcal{S}) - \boldsymbol{u}(\boldsymbol{x} \in \Omega^- \cap \mathcal{S})$ across it. In this case, the displacement field $\boldsymbol{u}(\boldsymbol{x})$ is expressed as

$$\boldsymbol{u}(\boldsymbol{x}) = \boldsymbol{u}^-(\boldsymbol{x}) + \mathscr{H}_{\mathcal{S}}(\boldsymbol{x})\, \hat{\boldsymbol{u}}(\boldsymbol{x}), \qquad \hat{\boldsymbol{u}}(\boldsymbol{x}) := \boldsymbol{u}^+(\boldsymbol{x}) - \boldsymbol{u}^-(\boldsymbol{x}) \tag{3.1a}$$

so that the strain field $\boldsymbol{\epsilon}(\boldsymbol{x})$ is given by

$$\boldsymbol{\epsilon}(\boldsymbol{x}) := \nabla^{\text{sym}}\boldsymbol{u}(\boldsymbol{x}) = \nabla^{\text{sym}}\boldsymbol{u}^-(\boldsymbol{x}) + \mathscr{H}_{\mathcal{S}}(\boldsymbol{x})\, \nabla^{\text{sym}}\hat{\boldsymbol{u}}(\boldsymbol{x}) + \big(\boldsymbol{w} \otimes \boldsymbol{n}\big)^{\text{sym}}\, \delta_{\mathcal{S}}(\boldsymbol{x}) \tag{3.1b}$$

where $\boldsymbol{u}^-(\boldsymbol{x})$ and $\boldsymbol{u}^+(\boldsymbol{x})$ denote the displacement fields in the parts Ω^- and Ω^+, respectively, with the former also representing the continuous displacement field in the solid Ω; $\hat{\boldsymbol{u}}(\boldsymbol{x}) : \Omega \to \mathbb{R}^{n_{\text{dim}}}$ signifies the relative displacement field of one part Ω^+ with respect to the other one Ω^-, satisfying the property $\hat{\boldsymbol{u}}(\boldsymbol{x} \in \mathcal{S}) = \boldsymbol{w}$; $\mathscr{H}_{\mathcal{S}}(\boldsymbol{x})$ is the Heaviside function defined at the interface $\mathcal{S}$, i.e., $\mathscr{H}_{\mathcal{S}}(\boldsymbol{x}) = 0$ if $\boldsymbol{x} \in \Omega^- \cup \mathcal{S}$ and $\mathscr{H}_{\mathcal{S}}(\boldsymbol{x}) = 1$ otherwise; $\delta_{\mathcal{S}}(\boldsymbol{x})$ denotes the Dirac-delta at the discontinuity $\mathcal{S}$.

The unbounded strain field (3.1b) resulting from the discontinuous displacement field (3.1a) can be regularized over a discontinuity band $\mathcal{B}$ of finite width b. Note that the width b is not a physical length but a regularization parameter which can be made as small as desired. As shown in Fig. 4(b), the regularized discontinuity (or discontinuity band) $\mathcal{B}$ is delimited by two surfaces $\mathcal{S}^+$ and $\mathcal{S}^-$ parallel to the discontinuity $\mathcal{S}$, i.e., $\Omega^+ \cup \Omega^- \cup \mathcal{B} = \Omega$. In this case, the displacement field $\boldsymbol{u}(\boldsymbol{x})$ is continuous, with an apparent displacement jump $\boldsymbol{w} := \boldsymbol{u}(\boldsymbol{x} \in \Omega^+ \cap \mathcal{S}^+) - \boldsymbol{u}(\boldsymbol{x} \in \Omega^- \cap \mathcal{S}^-)$ across the discontinuity band $\mathcal{B}$. Accordingly, the $\mathcal{C}^0$-continuous displacement field $\boldsymbol{u}(\boldsymbol{x})$ is expressed as [70, 71]

$$\boldsymbol{u}(\boldsymbol{x}) = \boldsymbol{u}^-(\boldsymbol{x}) + \mathscr{H}_{\mathcal{B}}(\boldsymbol{x})\, \hat{\boldsymbol{u}}(\boldsymbol{x}) \tag{3.2a}$$

and the singular strain field (3.1b) is regularized as

$$\boldsymbol{\epsilon}(\boldsymbol{x}) = \nabla^{\text{sym}}\boldsymbol{u}^{-}(\boldsymbol{x}) + \mathscr{H}_{\mathcal{B}}(\boldsymbol{x})\,\nabla^{\text{sym}}\hat{\boldsymbol{u}}(\boldsymbol{x}) + \big(\boldsymbol{e}\otimes\boldsymbol{n}\big)^{\text{sym}}\,\Xi_{\mathcal{B}}(\boldsymbol{x}) \tag{3.2b}$$

where the inelastic deformation vector $\boldsymbol{e} := \boldsymbol{w}/b$ is defined as the apparent displacement jump $\boldsymbol{w}$ normalized with respect to the band width b; $\mathscr{H}_{\mathcal{B}}(\boldsymbol{x})$ is a regularized ramp function defined as $\mathscr{H}_{\mathcal{B}}(\boldsymbol{x}) = 0$ if $\boldsymbol{x} \in \Omega^{-}$, $\mathscr{H}_{\mathcal{B}}(\boldsymbol{x}) = \frac{1}{b}\big(\boldsymbol{x} - \boldsymbol{x}^{*}\big)\cdot\boldsymbol{n}$ if $\boldsymbol{x} \in \mathcal{B}$ and $\mathscr{H}_{\mathcal{B}}(\boldsymbol{x}) = 1$ otherwise, with $\boldsymbol{x}^{*}$ being the spatial coordinates of point $\boldsymbol{x}$ projected along the direction $-\boldsymbol{n}$ to the surface $\mathcal{S}^{-}$; $\Xi_{\mathcal{B}}(\boldsymbol{x})$ denotes the collocation function within the discontinuity band $\mathcal{B}$, i.e., $\Xi_{\mathcal{B}}(\boldsymbol{x}) = 1$ if $\boldsymbol{x} \in \mathcal{B}$ and $\Xi_{\mathcal{B}}(\boldsymbol{x}) = 0$ otherwise.

For either the strong or regularized discontinuity, the strain field $\boldsymbol{\epsilon}(\boldsymbol{x})$ may be discontinuous across it, i.e.,

$$\boldsymbol{\epsilon}_{\mathcal{S}}^{+} - \boldsymbol{\epsilon}_{\mathcal{S}}^{-} = \nabla^{\text{sym}}\hat{\boldsymbol{u}}(\boldsymbol{x} \in \mathcal{S}) \tag{3.3}$$

where $\boldsymbol{\epsilon}_{\mathcal{S}}^{+} := \boldsymbol{\epsilon}(\boldsymbol{x} \in \Omega^{+} \cap \mathcal{S}^{+})$ and $\boldsymbol{\epsilon}_{\mathcal{S}}^{-} := \boldsymbol{\epsilon}(\boldsymbol{x} \in \Omega^{-} \cap \mathcal{S}^{-})$ represent the strains "ahead of" the surface $\mathcal{S}^{+}$ and "behind" the surface $\mathcal{S}^{-}$, respectively. Furthermore, once the discontinuity (band) forms, the strain $\boldsymbol{\epsilon}_{\mathcal{S}} := \boldsymbol{\epsilon}(\boldsymbol{x} \in \mathcal{S})$ at the discontinuity (band) always exhibits a jump with respect to the strain $\boldsymbol{\epsilon}_{\mathcal{S}}^{+}$ outside it, which verifies the Maxwell's compatibility condition

$$[\![\boldsymbol{\epsilon}]\!] := \boldsymbol{\epsilon}_{\mathcal{S}} - \boldsymbol{\epsilon}_{\mathcal{S}}^{+} = \big(\boldsymbol{e}\otimes\boldsymbol{n}\big)^{\text{sym}} = \frac{1}{b}\big(\boldsymbol{w}\otimes\boldsymbol{n}\big)^{\text{sym}} \tag{3.4}$$

Note that the strain jump $[\![\boldsymbol{\epsilon}]\!]$ is inversely proportional to b for a regularized discontinuity (or unbounded for a strong one).

In summary, the strong discontinuity $\mathcal{S}$ induces a discontinuous displacement field $\boldsymbol{u}(\boldsymbol{x})$ and a singular (unbounded) strain field $\boldsymbol{\epsilon}(\boldsymbol{x})$; see Fig. 5(a). Contrariwise, as shown in Fig. 5(b), the kinematic of a regularized discontinuity is characterized by a continuous displacement field $\boldsymbol{u}(\boldsymbol{x})$ and a regular (bounded) strain field $\boldsymbol{\epsilon}(\boldsymbol{x})$.

Remark 3.1 As the discontinuity band width b tends to zero, it follows that

$$\lim_{b\to 0}\mathscr{H}_{\mathcal{B}}(\boldsymbol{x}) = \mathscr{H}_{\mathcal{S}}(\boldsymbol{x}), \qquad \lim_{b\to 0}\frac{1}{b}\Xi_{\mathcal{B}}(\boldsymbol{x}) = \delta_{\mathcal{S}}(\boldsymbol{x}), \qquad \lim_{b\to 0}\boldsymbol{e}\,\Xi_{\mathcal{B}}(\boldsymbol{x}) = \boldsymbol{w}\delta_{\mathcal{S}}(\boldsymbol{x}) \tag{3.5}$$

That is, the strong discontinuity can be regarded as the limit of a regularized one, with a vanishing band width $b \to 0$. Reciprocally, a discontinuity band can be regarded as the convenient regularization of a strong discontinuity. □

Remark 3.2 In our previous work [12, 65, 66], it is assumed that the relative displacement field $\hat{\boldsymbol{u}}(\boldsymbol{x})$ is induced only by relative rigid body motions (e.g. translations and rotations) of one part Ω^{+} with respect to the other one Ω^{-} [62]. That is, its contribution to the strain field vanishes, i.e., $\nabla^{\text{sym}}\hat{\boldsymbol{u}}(\boldsymbol{x}) = \boldsymbol{0}$ and $\boldsymbol{\epsilon}_{\mathcal{S}}^{+} = \boldsymbol{\epsilon}_{\mathcal{S}}^{-}$. Accordingly, the strains at both sides of the discontinuity are continuous, though the relative displacement field $\hat{\boldsymbol{u}}(\boldsymbol{x})$ is not necessarily constant. This restrictive assumption is disregarded in the current work. □

3.2. Strain localization of softening solids

For strain localization to occur in a softening solid and to evolve eventually into a fully softened discontinuity at the final stage of the deformation process, material points inside the discontinuity (band) undergo inelastic loading

while those outside it unload elastically [10, 41]. That is, all the energy dissipative mechanisms (i.e., damage evolution and plastic flows of interest) are restricted to the discontinuity (band) during the subsequent failure process and do not develop further in the bulk. Owing to this fact and for the sake of simplicity, continuous inelastic strains prior to strain localization are neglected and only linear elastic bulk materials are considered in this work. However, this simplification does not preclude stiffness degradation and plastic strains resulting from continuous inelastic deformations prior to strain localization; see Remark 3.3 on this topic.

Upon strain localization, the following traction continuity condition has also to be fulfilled in addition to the classical equilibrium equations

$$\boldsymbol{\sigma}_{\mathcal{S}}^{+} \cdot \boldsymbol{n} = \boldsymbol{\sigma}_{\mathcal{S}}^{-} \cdot \boldsymbol{n} = \boldsymbol{t} \tag{3.6}$$

where the vector $\boldsymbol{t} := \boldsymbol{\sigma}_{\mathcal{S}} \cdot \boldsymbol{n}$ represents cohesive tractions at the discontinuity; $\boldsymbol{\sigma}_{\mathcal{S}}^{+} := \boldsymbol{\sigma}(\boldsymbol{x} \in \Omega^{+} \cap \mathcal{S})$, $\boldsymbol{\sigma}_{\mathcal{S}}^{-} := \boldsymbol{\sigma}(\boldsymbol{x} \in \Omega^{-} \cap \mathcal{S})$ and $\boldsymbol{\sigma}_{\mathcal{S}} := \boldsymbol{\sigma}(\boldsymbol{x} \in \mathcal{S})$ denote the stresses "ahead of", "behind" and "right" at the discontinuity (band), respectively. In accordance with the generic constitutive relations (2.8), they are determined as

$$\boldsymbol{\sigma}_{\mathcal{S}}^{+} = \mathbb{E}^{0} : \boldsymbol{\epsilon}_{\mathcal{S}}^{+}, \qquad \boldsymbol{\sigma}_{\mathcal{S}}^{-} = \mathbb{E}^{0} : \boldsymbol{\epsilon}_{\mathcal{S}}^{-} \tag{3.7a}$$

and

$$\boldsymbol{\sigma}_{\mathcal{S}} = \mathbb{E}^{0} : \left(\boldsymbol{\epsilon}_{\mathcal{S}} - \boldsymbol{\epsilon}_{\mathcal{S}}^{\text{in}}\right) \tag{3.7b}$$

As the bulk strains $\boldsymbol{\epsilon}_{\mathcal{S}}^{+}$ and $\boldsymbol{\epsilon}_{\mathcal{S}}^{-}$ at either side of the discontinuity $\mathcal{S}$ may be discontinuous, the resulting stresses, $\boldsymbol{\sigma}_{\mathcal{S}}^{+}$ and $\boldsymbol{\sigma}_{\mathcal{S}}^{-}$, may also be so.

Let us first consider the continuity between the tractions at both sides of the discontinuity, i.e.,

$$\left(\boldsymbol{\sigma}_{\mathcal{S}}^{+} - \boldsymbol{\sigma}_{\mathcal{S}}^{-}\right) \cdot \boldsymbol{n} = \boldsymbol{n} \cdot \mathbb{E}^{0} : \left(\boldsymbol{\epsilon}_{\mathcal{S}}^{+} - \boldsymbol{\epsilon}_{\mathcal{S}}^{-}\right) = \boldsymbol{0} \tag{3.8}$$

The general expression for the strain difference satisfying Eq. (3.8) is given by [4, 70]

$$\boldsymbol{\epsilon}_{\mathcal{S}}^{+} - \boldsymbol{\epsilon}_{\mathcal{S}}^{-} = \alpha_{mm} \boldsymbol{\Lambda}_{mm} + \alpha_{pp} \boldsymbol{\Lambda}_{pp} + \alpha_{mp} \boldsymbol{\Lambda}_{mp} \tag{3.9}$$

where a local orthogonal coordinate system $(\boldsymbol{n}, \boldsymbol{m}, \boldsymbol{p})$ is introduced at the discontinuity $\mathcal{S}$, with the tangential vectors $\boldsymbol{m}$ and $\boldsymbol{p}$ perpendicular to $\boldsymbol{n}$; the coefficients $(\alpha_{mm}, \alpha_{pp}, \alpha_{mp})$ and the second-order tensors $(\boldsymbol{\Lambda}_{mm}, \boldsymbol{\Lambda}_{pp}, \boldsymbol{\Lambda}_{mp})$ characterize the in-plane discontinuity modes (two relative stretching ones and a shear one) [70]

$$\boldsymbol{\Lambda}_{mm} := \boldsymbol{m} \otimes \boldsymbol{m} - \nu_0 \left(\boldsymbol{n} \otimes \boldsymbol{n} + \boldsymbol{p} \otimes \boldsymbol{p}\right) \tag{3.10a}$$

$$\boldsymbol{\Lambda}_{pp} := \boldsymbol{p} \otimes \boldsymbol{p} - \nu_0 \left(\boldsymbol{n} \otimes \boldsymbol{n} + \boldsymbol{m} \otimes \boldsymbol{m}\right) \tag{3.10b}$$

$$\boldsymbol{\Lambda}_{mp} := \left(\boldsymbol{m} \otimes \boldsymbol{p}\right)^{\text{sym}} \tag{3.10c}$$

with ν_0 being Poisson's ratio of the material. Note that the resulting stress field is not necessarily continuous, i.e., $\boldsymbol{\sigma}_{\mathcal{S}}^{+} \neq \boldsymbol{\sigma}_{\mathcal{S}}^{-}$, unless the condition $\alpha_{mm} = \alpha_{pp} = \alpha_{mp} = 0$ holds (or, equivalently, the relative displacement field $\hat{\boldsymbol{u}}(\boldsymbol{x})$

is caused only by the rigid body motions of the part Ω^+ with respect to the other one Ω^-). Accordingly, the restrictive stress continuity assumed in our previous work [63, 64, 66] is disregarded.

Similarly, the continuity between the tractions across the discontinuity can be expressed as

$$[\![\boldsymbol{t}]\!] = \left(\boldsymbol{\sigma}_{\mathcal{S}} - \boldsymbol{\sigma}_{\mathcal{S}}^{+}\right)\cdot\boldsymbol{n} = \boldsymbol{n}\cdot\mathbb{E}^{0} : \left[\left(\boldsymbol{e}\otimes\boldsymbol{n}\right)^{\mathrm{sym}} - \boldsymbol{\epsilon}_{\mathcal{S}}^{\mathrm{in}}\right] = \boldsymbol{0} \tag{3.11}$$

It then follows that

$$\left(\boldsymbol{e}\otimes\boldsymbol{n}\right)^{\mathrm{sym}} = \boldsymbol{\epsilon}_{\mathcal{S}}^{\mathrm{in}} + \left(\bar{\alpha}_{mm}\boldsymbol{\Lambda}_{mm} + \bar{\alpha}_{pp}\boldsymbol{\Lambda}_{pp} + \bar{\alpha}_{mp}\boldsymbol{\Lambda}_{mp}\right) \tag{3.12}$$

where the coefficients $(\bar{\alpha}_{mm}, \bar{\alpha}_{pp}, \bar{\alpha}_{mp})$ are not necessarily coincident with the ones $(\alpha_{mm}, \alpha_{pp}, \alpha_{mp})$ in Eq. (3.9).

On the one hand, in the kinematic relation (3.12) the second term of the right hand side is *elastic* and the coefficients $(\bar{\alpha}_{mm}, \bar{\alpha}_{pp}, \bar{\alpha}_{mp})$ are all independent of the band width b; otherwise, boundedness of the resulting stress field cannot be guaranteed. On the other hand, the remaining two terms in Eq. (3.12) are both inversely proportional to the bandwidth b for the regularized discontinuity (or even singular for the strong one); see Remark 2.2 and Eq. (3.4). Therefore, the kinematic relation (3.12) holds *if and only if the elastic item is canceled*, leading to

$$\boxed{[\![\boldsymbol{\epsilon}]\!] = \boldsymbol{\epsilon}_{\mathcal{S}}^{\mathrm{in}} = \left(\boldsymbol{e}\otimes\boldsymbol{n}\right)^{\mathrm{sym}} = \frac{1}{b}\left(\boldsymbol{w}\otimes\boldsymbol{n}\right)^{\mathrm{sym}}} \tag{3.13}$$

That is, upon strain localization in softening solids, *traction continuity along with stress boundedness* requires that ***the strain jump, defined as the difference in the strain fields between the interior/exterior points of the discontinuity (band) and characterized by Maxwell's compatibility condition, has to be completely inelastic***.

Remark 3.3 Inelastic deformations caused by, e.g., damage and plasticity, prior to strain localization can also be incorporated. In this context, the above problem can be regarded as inelastic discontinuities localized in an equivalent elastic medium with a damaged stiffness and some irreversible plastic strains, say $\bar{\mathbb{E}}$ and $\bar{\boldsymbol{\epsilon}}^{\mathrm{p}}$, respectively, which are both frozen once strain localization occurs in softening solids; see Fig. 6. Namely, one only needs to replace the linear elasticity tensor $\mathbb{E}^{0}$ by the fixed damaged bulk one $\bar{\mathbb{E}}$, and subtract the fixed bulk plastic strain $\bar{\boldsymbol{\epsilon}}^{\mathrm{p}}$ from the total one, while all the others remain unchanged. □

Remark 3.4 Note that the above novel strain localization, and in particular, the kinematic constraint (3.13), can also be written in rate form, but no additional insight in the problem is gained.

3.3. Application to the elastoplastic damage model

For the inelastic strain (2.9) in the elastoplastic damage model, upon strain localization the kinematic condition (3.13) is particularized as

$$\boldsymbol{\epsilon}^{\mathrm{in}} = \left(\boldsymbol{e}\otimes\boldsymbol{n}\right)^{\mathrm{sym}} = \boldsymbol{\epsilon}^{\mathrm{d}} + \boldsymbol{\epsilon}^{\mathrm{p}} \tag{3.14}$$

Recalling the recoverable/unrecoverable nature of the damage strain $\boldsymbol{\epsilon}^{\mathrm{d}}$ and the plastic one $\boldsymbol{\epsilon}^{\mathrm{p}}$, it follows that [65, 66]

$$\left(\boldsymbol{e}^{\mathrm{p}}\otimes\boldsymbol{n}\right)^{\mathrm{sym}} = \boldsymbol{\epsilon}^{\mathrm{p}} \tag{3.15a}$$

$$\left(\boldsymbol{e}^{\mathrm{d}}\otimes\boldsymbol{n}\right)^{\mathrm{sym}} = \boldsymbol{\epsilon}^{\mathrm{d}} = \mathbb{C}^{\mathrm{d}} : \boldsymbol{\sigma} \tag{3.15b}$$

where the damage and plastic deformation vectors, $\boldsymbol{e}^{\mathrm{d}} := \boldsymbol{w}^{\mathrm{d}}/b$ and $\boldsymbol{e}^{\mathrm{p}} := \boldsymbol{w}^{\mathrm{d}}/b$, are defined as the recoverable and unrecoverable displacement jumps $(\boldsymbol{w}^{\mathrm{d}}, \boldsymbol{w}^{\mathrm{p}})$ normalized with respect to the band width b. As only the nonlinear behavior of the discontinuity (band) is interested, the subscript '$_{\mathcal{S}}$' associated with the stress $\boldsymbol{\sigma}_{\mathcal{S}}$ is dropped here and subsequently for notational simplicity.

Eqs. (2.16a) and (3.15a) imply the existence of a *dissipative flow vector* $\boldsymbol{\gamma}$ satisfying

$$\boxed{\boldsymbol{\Lambda} = \big(\boldsymbol{\gamma} \otimes \boldsymbol{n}\big)^{\mathrm{sym}}} \tag{3.16}$$

or, equivalently [42],

$$\boldsymbol{\gamma} = 2\boldsymbol{n} \cdot \boldsymbol{\Lambda} - \boldsymbol{n}\Lambda_{nn} = \gamma_n \boldsymbol{n} + \gamma_m \boldsymbol{m} + \gamma_p \boldsymbol{p} \tag{3.17}$$

where the components $(\gamma_n, \gamma_m, \gamma_p)$ of the dissipative flow vector $\boldsymbol{\gamma}$ in the local orthogonal system $(\boldsymbol{n}, \boldsymbol{m}, \boldsymbol{p})$ are expressed as

$$\gamma_n := \boldsymbol{\gamma} \cdot \boldsymbol{n} = \Lambda_{nn}, \qquad \gamma_m := \boldsymbol{\gamma} \cdot \boldsymbol{m} = 2\Lambda_{nm}, \qquad \gamma_p := \boldsymbol{\gamma} \cdot \boldsymbol{p} = 2\Lambda_{np} \tag{3.18}$$

Substitution of the above dissipative flow vector $\boldsymbol{\gamma}$ into the relation (3.16) yields

$$\Lambda_{mm}(\boldsymbol{\theta}^{\mathrm{cr}}) = 0, \qquad \Lambda_{pp}(\boldsymbol{\theta}^{\mathrm{cr}}) = 0, \qquad \Lambda_{mp}(\boldsymbol{\theta}^{\mathrm{cr}}) = 0 \tag{3.19}$$

where $\boldsymbol{\theta}^{\mathrm{cr}}$ denote the characteristic discontinuity angles upon which the kinematic constraint (3.16) is satisfied. That is, all the dissipative flow components $(\Lambda_{mm}, \Lambda_{pp}, \Lambda_{mp})$ in the directions normal to the discontinuity (band) have to vanish.

3.4. Traction-based failure criterion

It follows from the constraints (3.19) that, upon strain localization the failure criterion $\mathcal{F}(\boldsymbol{\sigma}, q) \leq 0$ does not depend on the stress components $(\sigma_{mm}, \sigma_{pp}, \sigma_{mp})$, but is only a function of the tractions $\boldsymbol{t} = \big\{\sigma_{nn}, \sigma_{nm}, \sigma_{np}\big\}^{\mathrm{T}}$ acting on the discontinuity (band). Accordingly, provided the characteristic angles $\boldsymbol{\theta}^{\mathrm{cr}}$ satisfying the kinematic constraint (3.16) exist, it is alway possible to derive a traction-based failure criterion consistent with the given stress-based counterpart $\mathcal{F}(\boldsymbol{\sigma}, q) \leq 0$.

Let us consider the following stress-based failure function

$$\mathcal{F}(\boldsymbol{\sigma}, q) := \widehat{F}(\boldsymbol{\mathcal{I}}, q) \leq 0 \tag{3.20}$$

so that the dissipative flow tensor $\boldsymbol{\Lambda}$ is given by

$$\boldsymbol{\Lambda} = \widehat{\boldsymbol{\Lambda}} := \frac{\partial \widehat{F}}{\partial \boldsymbol{\sigma}} = \frac{\partial \widehat{F}}{\partial \sigma_1} \boldsymbol{v}_1 \otimes \boldsymbol{v}_1 + \frac{\partial \widehat{F}}{\partial I_1} \boldsymbol{I} + \frac{\partial \widehat{F}}{\partial J_2} \boldsymbol{s} + \cdots \tag{3.21}$$

where $\boldsymbol{\mathcal{I}} := \big\{\sigma_1, I_1, J_2, \cdots\big\}$ collects the invariants of the stress tensor $\boldsymbol{\sigma}$; $\sigma_1 := \boldsymbol{v}_1 \cdot \boldsymbol{\sigma} \cdot \boldsymbol{v}_1$ denotes the major principal stress, with $\boldsymbol{v}_1$ being the corresponding principal vector; $I_1 := \mathrm{tr}(\boldsymbol{\sigma})$ is the first invariant of the stress $\boldsymbol{\sigma}$, and $J_2 := \frac{1}{2}\boldsymbol{s} : \boldsymbol{s}$ represents the second invariant of the deviatoric stress $\boldsymbol{s} := \boldsymbol{\sigma} - \frac{1}{3}\mathrm{tr}(\boldsymbol{\sigma})\boldsymbol{I}$, respectively.

Accordingly, the relation (3.16) becomes

$$\boxed{\left(\boldsymbol{\gamma}\otimes\boldsymbol{n}\right)^{\mathrm{sym}}=\boldsymbol{\Lambda},\qquad \boldsymbol{\Lambda}=\widehat{\boldsymbol{\Lambda}}:=\frac{\partial\widehat{F}}{\partial\boldsymbol{\sigma}}}\tag{3.22}$$

If and only if the discontinuity orientation $\boldsymbol{n}(\boldsymbol{\theta}^{\mathrm{cr}})$ and the associated dissipative flow vector $\boldsymbol{\gamma}$ satisfying the kinematic constraint (3.22) exist for the given dissipative flow tensor $\widehat{\boldsymbol{\Lambda}}$, can the strong (or regularized) discontinuity forms upon strain localization in softening solids, and vice versa.

In this case, the orientation $\boldsymbol{n}(\boldsymbol{\theta}^{\mathrm{cr}})$ cannot be assumed arbitrarily as in the strong/regularized discontinuity approaches. But rather, it has to be determined from the kinematic constraints (3.19) for the given stress-based dissipative flow tensor $\boldsymbol{\Lambda}=\widehat{\boldsymbol{\Lambda}}$. On the one hand, as the set of equations is nonlinear, the solution may not exist at all. On the other hand, provided the solution exists, it depends only on the given failure criterion and the stress state, but not on the elastic properties (i.e., Poisson's ratio ν_0).

Once the discontinuity orientation $\boldsymbol{n}(\boldsymbol{\theta}^{\mathrm{cr}})$ is so determined, the corresponding dissipative flow vector $\boldsymbol{\gamma}$ can be obtained from Eqs. (3.17) and (3.18). Owing to the relation (3.24), the projected traction-based failure criterion $f(\boldsymbol{t},q)\leq 0$ can be determined as

$$f(\boldsymbol{t},q):=\widehat{F}(\boldsymbol{\sigma},q)=\frac{1}{M}\left(\widehat{\boldsymbol{\Lambda}}:\boldsymbol{\sigma}-\widehat{h}\cdot q\right)=\frac{1}{M}\left(\boldsymbol{\gamma}\cdot\boldsymbol{t}-\widehat{h}\cdot q\right)\leq 0\tag{3.23}$$

where the following identity

$$\boldsymbol{\Lambda}:\boldsymbol{\sigma}=\boldsymbol{\gamma}\cdot\left(\boldsymbol{\sigma}\cdot\boldsymbol{n}\right)=\boldsymbol{\gamma}\cdot\boldsymbol{t}\tag{3.24}$$

between the dissipative flow tensor $\boldsymbol{\Lambda}$ and the localized counterpart $\boldsymbol{\gamma}$ has been considered.

Remark 3.5 An alternative strategy is to introduce explicitly the traction-based failure criterion $\widehat{f}(\boldsymbol{t},q)\leq 0$, not necessarily coincident with the projected one (3.23), in an *ad hoc* manner. In such approaches [12], it is assumed *a priori* that the strong (or regularized) discontinuity can always form once strain localization occurs in solids. Accordingly, the kinematic constraint (3.16) automatically holds for any arbitrary orientation, such that it cannot be determined uniquely from the given traction-based failure criterion $\widehat{f}(\boldsymbol{t},q)\leq 0$, unless extra auxiliary conditions are introduced. In our previous work [12], the classical Mohr's maximization postulate [35] is adopted; see Appendix A for its relations to the kinematic constraints (3.19). The bi-directional connections and in particular, the equivalence conditions between these two strategies are referred to in Wu and Cervera [65, 66]. □

3.5. Localized plastic-damage model

Provided the characteristic angles $\boldsymbol{\theta}^{\mathrm{cr}}$ satisfying the kinematic constraint (3.16) exist, the damage evolution law (2.17) becomes

$$\dot{\mathbb{C}}=\dot{\mathbb{C}}^{\mathrm{d}}=\left(\dot{\boldsymbol{C}}^{\mathrm{d}}\,\overline{\otimes}\,\boldsymbol{N}\right)^{\mathrm{sym}}\qquad\Longrightarrow\qquad\mathbb{C}^{\mathrm{d}}=\left(\boldsymbol{C}^{\mathrm{d}}\,\overline{\otimes}\,\boldsymbol{N}\right)^{\mathrm{sym}}\tag{3.25}$$

for a second-order geometric tensor $\boldsymbol{N} := \boldsymbol{n} \otimes \boldsymbol{n}$. In other words, upon strain localization the damage behavior of the material is sufficiently characterized by a second-order compliance tensor $\boldsymbol{C}^{\mathrm{d}}$ with the evolution law

$$\dot{\boldsymbol{C}}^{\mathrm{d}} = \xi\, \lambda \frac{\boldsymbol{\gamma} \otimes \boldsymbol{\gamma}}{\boldsymbol{\gamma} \cdot \boldsymbol{t}} \tag{3.26}$$

where the identity (3.24) has been considered.

Accordingly, the damage strain tensor (3.15b) is given by

$$\boldsymbol{\epsilon}^{\mathrm{d}} = \left(\boldsymbol{e}^{\mathrm{d}} \otimes \boldsymbol{n}\right)^{\mathrm{sym}} = \left[\left(\boldsymbol{C}^{\mathrm{d}} \cdot \boldsymbol{t}\right) \otimes \boldsymbol{n}\right]^{\mathrm{sym}} \tag{3.27}$$

That is, the discontinuity (band) can be described by the following localized plastic-damage relations

$$\boldsymbol{e}^{\mathrm{d}} = \boldsymbol{e} - \boldsymbol{e}^{\mathrm{p}} = \boldsymbol{C}^{\mathrm{d}} \cdot \boldsymbol{t}, \qquad \boldsymbol{t} = \boldsymbol{E}^{\mathrm{d}} \cdot \boldsymbol{e}^{\mathrm{d}} = \boldsymbol{E}^{\mathrm{d}} \cdot \left(\boldsymbol{e} - \boldsymbol{e}^{\mathrm{p}}\right) \tag{3.28a}$$

$$\dot{\boldsymbol{e}}^{\mathrm{p}} = \left(1 - \xi\right)\lambda \boldsymbol{\gamma} \tag{3.28b}$$

for the second-order stiffness tensor $\boldsymbol{E}^{\mathrm{d}} := \left(\boldsymbol{C}^{\mathrm{d}}\right)^{-1}$.

By time differentiation, the rate constitutive relations are expressed as

$$\dot{\boldsymbol{t}} = \boldsymbol{E}^{\mathrm{d}} \cdot \left(\dot{\boldsymbol{e}} - \dot{\boldsymbol{e}}^{\mathrm{dis}}\right), \qquad \dot{\boldsymbol{e}} = \boldsymbol{C}^{\mathrm{d}} \cdot \dot{\boldsymbol{t}} + \dot{\boldsymbol{e}}^{\mathrm{dis}} \tag{3.29}$$

where the *dissipative deformation vector rate* $\dot{\boldsymbol{e}}^{\mathrm{dis}}$ is defined as

$$\dot{\boldsymbol{e}}^{\mathrm{dis}} := \dot{\boldsymbol{C}}^{\mathrm{d}} \cdot \boldsymbol{t} + \dot{\boldsymbol{e}}^{\mathrm{p}} = \lambda \boldsymbol{\gamma} \qquad \Longrightarrow \qquad \left(\dot{\boldsymbol{e}}^{\mathrm{dis}} \otimes \boldsymbol{n}\right)^{\mathrm{sym}} = \dot{\boldsymbol{\epsilon}}^{\mathrm{dis}} = \lambda \boldsymbol{\Lambda} \tag{3.30}$$

with $\dot{\boldsymbol{C}}^{\mathrm{d}} \cdot \boldsymbol{t}$ and $\dot{\boldsymbol{e}}^{\mathrm{p}}$ being its damage and plastic components, respectively; see Fig. 7.

Owing to the relation (3.24), upon strain localization the multiplier $\lambda > 0$ for an active discontinuity band can be determined in terms of the inelastic deformation vector $\boldsymbol{e}$ rather than the strain tensor $\boldsymbol{\epsilon}$ as in Eq. (2.18), i.e.,

$$\lambda = \frac{\boldsymbol{\gamma} \cdot \boldsymbol{E}^{\mathrm{d}} \cdot \dot{\boldsymbol{e}}}{\boldsymbol{\gamma} \cdot \boldsymbol{E}^{\mathrm{d}} \cdot \boldsymbol{\gamma} + h \cdot H \cdot h} = \frac{\boldsymbol{\gamma} \cdot \dot{\boldsymbol{t}}}{h \cdot H \cdot h} \tag{3.31}$$

Combination of Eqs. (3.29), (3.30) and (3.31) yields the following rate constitutive relations

$$\dot{\boldsymbol{t}} = \boldsymbol{E}^{\mathrm{d}} \cdot \left(\dot{\boldsymbol{e}} - \lambda \boldsymbol{\gamma}\right) = \boldsymbol{E}^{\mathrm{d}}_{\mathrm{tan}} \cdot \dot{\boldsymbol{e}}, \qquad \dot{\boldsymbol{e}} = \boldsymbol{C}^{\mathrm{d}} \cdot \dot{\boldsymbol{t}} + \lambda \boldsymbol{\gamma} = \boldsymbol{C}^{\mathrm{d}}_{\mathrm{tan}} \cdot \dot{\boldsymbol{t}} \tag{3.32}$$

where the tangent stiffness $\boldsymbol{E}^{\mathrm{d}}_{\mathrm{tan}}$ and compliance $\boldsymbol{C}^{\mathrm{d}}_{\mathrm{tan}}$ are expressed as

$$\boldsymbol{E}^{\mathrm{d}}_{\mathrm{tan}} = \boldsymbol{E}^{\mathrm{d}} - \frac{\boldsymbol{E}^{\mathrm{d}} \cdot \left(\boldsymbol{\gamma} \otimes \boldsymbol{\gamma}\right) \cdot \boldsymbol{E}^{\mathrm{d}}}{\boldsymbol{\gamma} \cdot \boldsymbol{E}^{\mathrm{d}} \cdot \boldsymbol{\gamma} + h \cdot H \cdot h} \tag{3.33a}$$

$$\boldsymbol{C}^{\mathrm{d}}_{\mathrm{tan}} = \boldsymbol{C}^{\mathrm{d}} + \frac{\boldsymbol{\gamma} \otimes \boldsymbol{\gamma}}{h \cdot H \cdot h} \tag{3.33b}$$

for the active discontinuity (band).

Therefore, ***provided the kinematic constraint resulting from the traction continuity along with stress boundedness is fulfilled, consistent traction-based constitutive relations for the discontinuity (band) naturally emerges from the strain localization analysis of stress-based models with regularized softening regime***.

Remark 3.6 For the damage compliance tensor $\mathbb{C}^{\mathrm{d}}$ in Eq. (3.25)$_2$, the (complementary) damage free energy density function ψ^{d} introduced in Eq. (2.11b) localizes within the discontinuity (band), i.e.,

$$\psi^{\mathrm{d}} = \frac{1}{2}\boldsymbol{\sigma} : \mathbb{C}^{\mathrm{d}} : \boldsymbol{\sigma} = \frac{1}{2}\boldsymbol{t} \cdot \boldsymbol{C}^{\mathrm{d}} \cdot \boldsymbol{t} = \frac{1}{2}\boldsymbol{e}^{\mathrm{d}} \cdot \boldsymbol{E}^{\mathrm{d}} \cdot \boldsymbol{e}^{\mathrm{d}} \tag{3.34}$$

Similarly, the energy dissipation (2.12) becomes

$$\mathscr{D} = \frac{1}{2}\,\boldsymbol{t} \cdot \dot{\boldsymbol{C}}^{\mathrm{d}} \cdot \boldsymbol{t} + \boldsymbol{t} \cdot \dot{\boldsymbol{e}}^{\mathrm{p}} + \left(q^0 - q\right) \cdot \dot{\kappa} \geq 0 \tag{3.35}$$

Accordingly, the above localized plastic-damage model can also be derived by making standard arguments [65]. In particular, the material compliance $\mathbb{C}$ can be related to the discontinuity (band) compliance $\boldsymbol{C}^{\mathrm{d}}$ as follows

$$\mathbb{C} = \mathbb{C}^0 + \mathbb{C}^{\mathrm{d}} = \mathbb{C}^0 + \left(\boldsymbol{C}^{\mathrm{d}} \,\overline{\otimes}\, \boldsymbol{N}\right)^{\mathrm{sym}} \tag{3.36a}$$

Inversely, the material stiffness tensor $\mathbb{E}$ is obtained from the Sherman-Morrison-Woodburg formula [20]

$$\mathbb{E} = \mathbb{C}^{-1} = \mathbb{E}^0 - \mathbb{E}^0 : \left[\left(\boldsymbol{E}^{\mathrm{d}} + \boldsymbol{n} \cdot \mathbb{E}^0 \cdot \boldsymbol{n}\right)^{-1} \overline{\otimes}\, \boldsymbol{N}\right]^{\mathrm{sym}} : \mathbb{E}^0 \tag{3.36b}$$

Note that both the material compliance $\mathbb{C}$ and stiffness $\mathbb{E}$ are symmetric. □

Remark 3.7 In the above localized plastic-damage model, the *strain-like* internal variable κ is employed in the softening law $q(\kappa)$. Accordingly, the resulting localized constitutive laws are expressed in terms of the traction $\boldsymbol{t}$ and the inelastic deformation vector $\boldsymbol{e}$. Recalling the relations (2.23), the equivalent localized model in terms of tractions $\boldsymbol{t}$ *versus* displacement jumps $\boldsymbol{w}$ can also be developed. The details are omitted here. □

4. Plane stress and plane strain cases

In this section let us analyze the 2D cases of plane stress and plane strain. As shown in Fig. 8, a solid $\Omega \subset \mathbb{R}^2$ with a discontinuity $\mathcal{S}$ is considered. The in-plane principal stresses are denoted by σ_1 and σ_2 ($\sigma_1 \geq \sigma_2$), respectively, while the third one σ_3 is orthogonal to that plane. In such 2D cases the discontinuity orientation can be characterized by the inclination angle (anti-clockwise) $\theta \in [-\pi/2, \pi/2]$ between the normal vector $\boldsymbol{n}$ and the principal vector $\boldsymbol{v}_1$ of the stress tensor. The tangential vectors $\boldsymbol{m}$ and $\boldsymbol{p}$ of the discontinuity $\mathcal{S}$ are located on and perpendicular to the plane of interest, respectively.

The task is to derive explicitly the discontinuity angle θ^{cr} and the traction-based failure criterion $f(\boldsymbol{t}, q) \leq 0$ projected from the given stress-based counterpart $\widehat{F}(\boldsymbol{\sigma}, q) \leq 0$. Several classical failure criteria, i.e., Rankine, Mohr-Coulomb, von Mises and Drucker-Prager models, are considered; see Wu and Cervera [65] for more general ones.

4.1. Discontinuity angle

For a given stress-based failure criterion $\widehat{F}(\boldsymbol{\sigma}, q) \leq 0$, the discontinuity angle θ^{cr} can be determined explicitly through the projection relation (3.22) or more specifically, through Eqs. (3.19), i.e.,

$$\widehat{\Lambda}_{mm}(\theta^{\mathrm{cr}}) = 0, \qquad \widehat{\Lambda}_{pp}(\theta^{\mathrm{cr}}) = 0 \tag{4.1}$$

Note that in 2D cases the last constraint $\widehat{\Lambda}_{mp}(\theta^{\mathrm{cr}}) = 0$ is automatically satisfied.

It follows from the Mohr's circle and the constraint $\widehat{\Lambda}_{mm}(\theta^{\mathrm{cr}}) = 0$ that [65, 66]

$$\sin^2\theta^{\mathrm{cr}} = -\frac{\widehat{\Lambda}_2}{\widehat{\Lambda}_1 - \widehat{\Lambda}_2}, \qquad \cos^2\theta^{\mathrm{cr}} = \frac{\widehat{\Lambda}_1}{\widehat{\Lambda}_1 - \widehat{\Lambda}_2} \tag{4.2}$$

where $\widehat{\Lambda}_1$ and $\widehat{\Lambda}_2$ (assuming $\widehat{\Lambda}_1 \geq \widehat{\Lambda}_2$ as usual) denote the principle values of the dissipative flow tensor $\boldsymbol{\Lambda}$. The above results apply upon the conditions $\widehat{\Lambda}_1 \geq 0$ and $\widehat{\Lambda}_2 \leq 0$; see Appendix B for the exceptional cases.

Obviously, the discontinuity angle θ^{cr} depends on the ratio $\widehat{\Lambda}_2/\widehat{\Lambda}_1$ or, equivalently, the stress state upon strain localization. Regarding the remaining condition, $\widehat{\Lambda}_{pp} = 0$, the conditions of plane stress and plane strain have to be discriminated.

4.1.1. Plane stress

In the case of plane stress, the out-of-plane stress component $\sigma_{pp} = \sigma_3 = 0$ vanishes such that the corresponding dissipative flow component $\widehat{\Lambda}_{pp} = \widehat{\Lambda}_3 = 0$ needs not be considered. Therefore, once the initial failure surface is reached, i.e., $\widehat{F}(\boldsymbol{\sigma}, q^0) = 0$, the strong (or regularized) discontinuity forms at the same instant, with the orientation determined from Eqs. (4.2).

Note that in the case of plane stress, for the material model with associated evolution laws the discontinuity angle θ^{cr} determined from Eqs. (4.2) coincides with that obtained from the classical discontinuous bifurcation analysis [53].

4.1.2. Plane strain

In the case of plane strain (i.e. $\epsilon_3 = 0$), on the one hand, the elastic out-of-plane stress σ_3 is given by

$$\sigma_3 = \nu_0(\sigma_1 + \sigma_2) \tag{4.3}$$

On the other hand, for the homogeneous loading function $\hat{F}(\boldsymbol{\sigma}, q)$ of degree $M \leq 2$, the condition $\widehat{\Lambda}_{pp} = 0$ gives

$$\widehat{\Lambda}_{pp} = \widehat{\Lambda}_3 = 0 \qquad \Longrightarrow \qquad \sigma_3 = \eta_1(\sigma_1 + \sigma_2) + \eta_2 q \tag{4.4}$$

where η_1 and η_2 are related to the parameters involved in the specified stress-based failure criterion $\hat{F}(\boldsymbol{\sigma}, q) \leq 0$; see the examples presented later. As the in-plane principal values $\widehat{\Lambda}_1$ and $\widehat{\Lambda}_2$ depend on the out-of-plane stress $\sigma_3 \neq 0$, the discontinuity angle θ^{cr}, still determined from Eq. (4.2), is affected by this extra plane strain localization condition.

The out-of-plane stress (4.4), necessary for plane strain localization, is in general different from the elastic value (4.3). Furthermore, the initial limit surface $\widehat{F}(\boldsymbol{\sigma}, q^0) = 0$ will be reached earlier with the elastic out-of-plane stress (4.3) than with the localized one (4.4). Accordingly, except for very particular cases, strain localization cannot occur at the onset of softening. Rather, some (continuous) inelastic deformations and substantial rotation of the principal strain directions have to occur first at the beginning of the softening regime, until the plane strain localization condition (4.4) is fulfilled. From that moment on, the (continuous) inelastic deformations in the bulk material are frozen (unloading), and the discontinuous inelastic deformations within the discontinuity (band) continue growing due to strain localization. That is, the bulk material is considered as linear elastic after strain localization occurs, however, with degraded

(unloading) stiffness and plastic deformations corresponding to those at the time when strain localization is initiated. The above delayed strain localization in the plane strain condition, similarly to the transited continuous-discontinuous failure [30] illustrated in Fig. 9, was numerically observed in Cervera et al. [10] for von Mises (J_2) model. As shown in Section 4.6, it also occurs for other failure criteria like the classical Drucker-Prager model.

4.2. *Traction-based failure criterion*

With the discontinuity angle $\theta^{\rm cr}$ determined from Eq. (4.2), the normal and tangent components (γ_n, γ_m) of the dissipative flow vector $\boldsymbol{\gamma}$ are given by

$$\gamma_n = \widehat{\Lambda}_{nn}(\theta^{\rm cr}) = \big(\widehat{\Lambda}_1 - \widehat{\Lambda}_2\big)\cos(2\theta^{\rm cr}) = \widehat{\Lambda}_1 + \widehat{\Lambda}_2 \tag{4.5a}$$

$$\gamma_m = 2\widehat{\Lambda}_{nm}(\theta^{\rm cr}) = \big(\widehat{\Lambda}_1 - \widehat{\Lambda}_2\big)\sin(2\theta^{\rm cr}) = 2\text{sign}(\sigma_{nm})\sqrt{-\widehat{\Lambda}_1\widehat{\Lambda}_2} \tag{4.5b}$$

with $\text{sign}(\cdot)$ being the sign function.

In accordance with Eq. (3.23), the stress-based failure criterion $\widehat{F}(\boldsymbol{\sigma}, q) \le 0$ is projected to the orientation $\boldsymbol{n}(\theta^{\rm cr})$ as the following traction-based counterpart

$$f(\boldsymbol{t}, q) = \frac{1}{M}\Big[\big(\widehat{\Lambda}_1 + \widehat{\Lambda}_2\big)t_n + 2\sqrt{-\widehat{\Lambda}_1\widehat{\Lambda}_2}\,|t_m| - \widehat{h}\cdot q\Big] \le 0 \tag{4.6}$$

Similarly, the projected traction-based failure criterion (4.6) holds for the cases $\widehat{\Lambda}_1 \ge 0$ and $\widehat{\Lambda}_2 \le 0$; the exceptional cases are also dealt with in Appendix B.

Remark 4.1 For the projected traction-based failure criterion (4.6), its first- and second-order derivatives with respect to θ read

$$\frac{\partial f}{\partial \theta} = -\frac{1}{2}(\sigma_1 - \sigma_2)\Big[\big(\widehat{\Lambda}_1 + \widehat{\Lambda}_2\big) - \big(\widehat{\Lambda}_1 - \widehat{\Lambda}_2\big)\cos(2\theta)\Big]\sin(2\theta) \tag{4.7a}$$

$$\frac{\partial^2 f}{\partial \theta^2} = -(\sigma_1 - \sigma_2)\Big[\big(\widehat{\Lambda}_1 + \widehat{\Lambda}_2\big)\cos(2\theta) - \big(\widehat{\Lambda}_1 - \widehat{\Lambda}_2\big)\cos(4\theta)\Big] \tag{4.7b}$$

For the discontinuity angle $\theta^{\rm cr}$ given from Eq. (4.2), it follows that

$$\left.\frac{\partial f}{\partial \theta}\right|_{\theta^{\rm cr}} = 0, \qquad \left.\frac{\partial^2 f}{\partial \theta^2}\right|_{\theta^{\rm cr}} < 0 \tag{4.8}$$

Therefore, provided strain localization can occur, the tractions (t_n, t_m) do maximize the projected traction-based failure criterion $f(\boldsymbol{t}, q) \le 0$. ■

4.3. *Example: Rankine criterion*

The Rankine criterion, widely adopted for the modeling of tensile failure in quasi-brittle materials, is expressed in terms of the major principal stress $\sigma_1 = \boldsymbol{v}_1 \cdot \boldsymbol{\sigma} \cdot \boldsymbol{v}_1 > 0$ as

$$\widehat{F}(\boldsymbol{\sigma}, q) = \langle\sigma_1\rangle - q = \mathscr{H}(\sigma_1)\,\sigma_1 - q \le 0 \tag{4.9}$$

where the Macaulay brackets $\langle\cdot\rangle$ and Heaviside function $\mathscr{H}(\cdot)$ are defined as: $\langle x\rangle = x$, $\mathscr{H}(x) = 1$ if $x > 0$, and $\langle x\rangle = 0$, $\mathscr{H}(x) = 0$ otherwise, respectively.

In both plane stress and plane strain conditions, it follows from Eq. (4.2) that

$$\sin^2\theta^{\mathrm{cr}} = 0 \qquad \Longrightarrow \qquad \theta^{\mathrm{cr}} = 0 \tag{4.10}$$

As expected, only a mode I discontinuity (in the context of fracture mechanics) can be initiated. With the discontinuity angle (4.10), the traction-based failure criterion (4.6) becomes

$$f(\boldsymbol{t}, q) = \mathscr{H}(\sigma_1)t_n - q = \langle t_n\rangle - q \le 0 \tag{4.11}$$

where the relation $\sigma_1 = \boldsymbol{n}\cdot\boldsymbol{\sigma}\cdot\boldsymbol{n} = t_n$ has been considered for mode-I failure.

4.4. Example: Mohr-Coulomb criterion

Let us then consider the Mohr-Coulomb criterion, with the failure function defined as

$$\widehat{F}(\boldsymbol{\sigma}, q) = \begin{cases} \frac{1}{2}\Big[\big(\sigma_1+\sigma_3\big)\sin\varphi + \big(\sigma_1-\sigma_3\big)\Big] - q\cos\varphi & \text{Region 1}: \sigma_1 \ge \sigma_2 \ge \sigma_3 \\ \frac{1}{2}\Big[\big(\sigma_1+\sigma_2\big)\sin\varphi + \big(\sigma_1-\sigma_2\big)\Big] - q\cos\varphi & \text{Region 2}: \sigma_1 \ge \sigma_3 \ge \sigma_2 \\ \frac{1}{2}\Big[\big(\sigma_3+\sigma_2\big)\sin\varphi + \big(\sigma_3-\sigma_2\big)\Big] - q\cos\varphi & \text{Region 3}: \sigma_3 \ge \sigma_1 \ge \sigma_2 \end{cases} \tag{4.12}$$

where the internal friction angle $\varphi \in [0, \pi/2]$ is determined from

$$\sin\varphi = \frac{\rho-1}{\rho+1} \qquad \Longleftrightarrow \qquad \rho = \frac{1+\sin\varphi}{1-\sin\varphi} \tag{4.13}$$

for the ratio $\rho := f_c/f_t \ge 1$ between the uniaxial compressive strength f_c and the tensile one f_t.

In the case of plane stress ($\sigma_3 = 0$), it follows from Eq. (4.2) that $\theta^{\mathrm{cr}} = 0$ in Region 1 and $\theta^{\mathrm{cr}} = \pi/2$ in Region 3, respectively; in Region 2 (i.e., $\sigma_1 \ge \sigma_3 \ge \sigma_2$), the discontinuity angle θ^{cr} is determined as

$$\sin^2\theta^{\mathrm{cr}} = \frac{1}{2}\big(1-\sin\varphi\big) \qquad \Longrightarrow \qquad \theta^{\mathrm{cr}} = \pm\Big(\frac{\pi}{4} - \frac{\varphi}{2}\Big) \tag{4.14}$$

The above results coincide with those obtained from Mohr's maximization postulate.

In the case of plane strain, the extra constraint $\widehat{\Lambda}_3 = 0$ cannot be satisfied in Regions 1 and 3; only in Region 2 (i.e., $\sigma_1 \ge \sigma_3 \ge \sigma_2$) can strain localization occur, with the same discontinuity angle (4.14).

For the discontinuity angle (4.14), in Region 2 ($\sigma_1 \ge \sigma_3 \ge \sigma_2$) the traction-based failure criterion (4.5) reads

$$f(\boldsymbol{t}, q) = \cos\varphi\Big(t_n\tan\varphi + \big|t_m\big| - q\Big) \le 0 \tag{4.15a}$$

or, equivalently,

$$\tan\varphi\cdot t_n + \big|t_m\big| - q \le 0 \tag{4.15b}$$

in both cases of plane stress and plane strain. This is exactly the classical traction-based Mohr-Coulomb criterion.

Remark 4.2 Tresca's criterion is recovered for the friction angle $\varphi = 0$ in the Mohr-Coulomb criterion (4.12). In Region 2 ($\sigma_1 \geq \sigma_3 \geq \sigma_2$), the discontinuity angle is then $\theta^{\rm cr} = \pi/4$, and the corresponding traction-based failure criterion is expressed as

$$f(\boldsymbol{t}, q) = \left|t_m\right| - q \leq 0 \tag{4.16}$$

for both cases of plane stress and plane strain. ■

4.5. Example: von Mises (J_2) criterion

The von Mises (J_2) criterion is now considered

$$\hat{F}(\boldsymbol{\sigma}, q) = \sqrt{3J_2} - q = \sqrt{\frac{3}{2}}\left\|\boldsymbol{s}\right\| - q \leq 0 \tag{4.17}$$

in terms of the second invariant $J_2 := \frac{1}{2}\boldsymbol{s} : \boldsymbol{s}$ or the norm $\left\|\boldsymbol{s}\right\| := \boldsymbol{s} : \boldsymbol{s}$ of the deviatoric stress tensor $\boldsymbol{s}$.

The discontinuity angle $\theta^{\rm cr}$ is given from Eq. (4.2) as

$$\sin^2\theta^{\rm cr} = -\frac{s_2}{s_1 - s_2}, \qquad \cos^2\theta^{\rm cr} = \frac{s_1}{s_1 - s_2} \tag{4.18}$$

for the in-plane principal values s_i $(i = 1, 2)$ of the deviatoric stress tensor $\boldsymbol{s}$.

4.5.1. Plane stress

In the case of plane stress ($\sigma_3 = 0$), it follows that

$$\sin^2\theta^{\rm cr} = \frac{\sigma_1 - 2\sigma_2}{3(\sigma_1 - \sigma_2)}, \qquad \cos^2\theta^{\rm cr} = \frac{2\sigma_1 - \sigma_2}{3(\sigma_1 - \sigma_2)} \tag{4.19}$$

if the conditions $\sigma_1 \geq \frac{1}{2}\sigma_2$ and $\sigma_1 \geq 2\sigma_2$ are satisfied. The resulting discontinuity angles $\theta^{\rm cr}$ for different stress ratios σ_1/σ_2 are summarized in Table 1 and depicted in Fig. 10.

Table 1: Discontinuity angles $\theta^{\rm cr}$ for the von Mises criterion in the condition of plane stress

	Stress ratio σ_1/σ_2							
	-1: -2	-1: -5	0: -1	1: -5	1: -1	1: 0	1: 0.25	1: 0.5
$\theta^{\rm cr}$	90.00°	60.00°	54.74°	51.42°	45.00°	35.26°	28.12°	0.00°

With the discontinuity angle (4.19), the corresponding normal and tangential tractions (t_n, t_m) are evaluated as

$$t_n = \sigma_{nn} = \frac{2}{3}(\sigma_1 + \sigma_2), \qquad t_m^2 = \sigma_{nm}^2 = -s_1 s_2 \tag{4.20}$$

so that

$$J_2 = \frac{1}{3}(\sigma_1^2 + \sigma_2^2 - \sigma_1\sigma_2) = \frac{1}{4}t_n^2 + t_m^2 \tag{4.21}$$

Substitution of the result (4.21) into Eq. (4.17) yields the following traction-based failure function

$$f(\boldsymbol{t},q) = \sqrt{3\Big(\frac{1}{4}t_n^2 + t_m^2\Big)} - q \le 0 \tag{4.22}$$

The above failure criterion can also be derived from the definition (4.6). For the equi-biaxial tension/compression stress state, i.e., $\sigma_2 = -\sigma_1$ and $t_n = 0$, the expected pure shear failure criterion is recovered.

Remark 4.3 For the cases $\sigma_1 \le \frac{1}{2}\sigma_2$ or $\sigma_1 \le 2\sigma_2$, the discontinuity angle $\theta^{\rm cr}$ in Eq. (B.1) applies. Accordingly, the modified stress- and traction-based failure criteria are given from Eqs. (B.2) and (B.3), respectively, i.e.,

$$\widehat{F}(\boldsymbol{\sigma},q) = \begin{cases} \dfrac{\sqrt{3}}{2}\sigma_1 - q & 0 < \sigma_2 < \sigma_1 < 2\sigma_2 \\ -\dfrac{\sqrt{3}}{2}\sigma_2 - q & 2\sigma_1 < \sigma_2 < \sigma_1 < 0 \end{cases} \tag{4.23a}$$

$$f(\boldsymbol{t},q) = \frac{\sqrt{3}}{2}\big|t_n\big| - q \le 0 \tag{4.23b}$$

The above modified failure criteria with tension- and compression-extensions are also illustrated in Fig. 10. ■

4.5.2. Plane strain

In the case of plane strain, the condition (4.4) requires that

$$\widehat{\Lambda}_3 = 0 \qquad \Longrightarrow \qquad s_3 = 0, \qquad \sigma_3 = \frac{1}{2}(\sigma_1 + \sigma_2) \tag{4.24}$$

That is, $\eta_1 = 1/2$ and $\eta_2 = 0$ in the out-of-plane principal stress (4.4).

Upon the above stress state, it follows that $s_1 = -s_2$ such that the discontinuity angle $\theta^{\rm cr}$ is determined from Eq. (4.18) as

$$\sin^2\theta^{\rm cr} = -\frac{s_2}{s_1 - s_2} = \frac{1}{2} \qquad \Longrightarrow \qquad \theta^{\rm cr} = 45^\circ \tag{4.25}$$

As can be seen, in the condition of plane strain the discontinuity angle is fixed as $\theta^{\rm cr} = 45^\circ$ independently of the stress ratio σ_1/σ_2. Note that the above result, recently confirmed by the numerical simulations [10], is different from that given from the discontinuous bifurcation analysis [53].

For the discontinuity angle (4.25), the traction-based failure function (4.6) is expressed as

$$f(\boldsymbol{t},q) = \sqrt{3}\,\big|t_m\big| - q \le 0 \tag{4.26}$$

As expected, for the von Mises criterion in the plane strain condition a pure mode II discontinuity forms upon strain localization, whatever the stress state is.

Remark 4.4 In the case of plane strain, with the elastic out-of-plane stress (4.3) the initial elastic limit surface $\widehat{F}(\boldsymbol{\sigma},q^0) = 0$ is expressed as

$$\sqrt{(1 - \nu_0 + \nu_0^2)(\sigma_1^2 + \sigma_2^2) - (1 + 2\nu_0 - 2\nu_0^2)\sigma_1\sigma_2} = q^0 \tag{4.27}$$

Contrariwise, with the out-of-plane stress (4.24) upon plane strain localization, the failure criterion $\widehat{F}(\boldsymbol{\sigma}, q) \leq 0$ becomes two parallel straight lines, i.e.,

$$\widehat{F}(\boldsymbol{\sigma}, q) = \frac{\sqrt{3}}{2} \left|\sigma_1 - \sigma_2\right| - q \leq 0 \tag{4.28}$$

As depicted in Fig. 11, only for the particular cases $\nu_0 = 0.5$ or $\sigma_2 = -\sigma_1$, can strain localization occur at the onset of strain softening. For all other cases, the elastic limit surface (4.27) will be reached first and strain softening occurs accompanied with (continuous) inelastic deformations. Only when sufficient re-orientation of the principal strain directions is completed so that the plane strain localization condition (4.24) is fulfilled, strain localization sets in motion and a strong (regularized) discontinuity forms. ■

4.6. Example: Drucker-Prager criterion

Finally, let us consider the Drucker-Prager criterion expressed as

$$\widehat{F}(\boldsymbol{\sigma}, q) = \frac{1}{1+\alpha}\Big(\alpha I_1 + \sqrt{3J_2}\Big) - q \leq 0 \tag{4.29}$$

where the parameter $\alpha = (\rho - 1)/(\rho + 1) \in [0, 1)$ is related to the ratio $\rho := f_c/f_t \geq 1$ between the uniaxial compressive strength f_c and the tensile one f_t.

The discontinuity angle θ^{cr} is computed from Eq. (4.2) as

$$\sin^2\theta^{\text{cr}} = -\frac{\sqrt{2/3}\,\alpha\|\boldsymbol{s}\| + s_2}{s_1 - s_2}, \qquad \cos^2\theta^{\text{cr}} = \frac{\sqrt{2/3}\,\alpha\|\boldsymbol{s}\| + s_1}{s_1 - s_2} \tag{4.30}$$

where s_1 and s_2 denote the in-plane principal values of the deviatoric stress tensor $\boldsymbol{s}$.

Remark 4.5 For an activated discontinuity, it follows from the fact $\widehat{F}(\boldsymbol{\sigma}, q) = 0$ that

$$\sqrt{\frac{2}{3}}\,\|\boldsymbol{s}\| = \frac{2}{3}\Big[(1+\alpha)q - \alpha I_1\Big] \geq 0 \tag{4.31}$$

This relation is useful for later derivation of the traction-based failure criterion $f(\boldsymbol{t}, q) \leq 0$. □

4.6.1. Plane stress

In the case of plane stress ($\sigma_3 = 0$), it follows from Eq. (4.30) that

$$\sin^2\theta^{\text{cr}} = -\frac{(2\sigma_2 - \sigma_1) + 2\alpha\sqrt{\sigma_1^2 + \sigma_2^2 - \sigma_1\sigma_2}}{3(\sigma_1 - \sigma_2)} \tag{4.32a}$$

$$\cos^2\theta^{\text{cr}} = \frac{(2\sigma_1 - \sigma_2) + 2\alpha\sqrt{\sigma_1^2 + \sigma_2^2 - \sigma_1\sigma_2}}{3(\sigma_1 - \sigma_2)} \tag{4.32b}$$

if the conditions $\sigma_1 \geq \widetilde{\alpha}_1\sigma_2$ and $\sigma_1 \geq \sigma_2/\widetilde{\alpha}_2$ are satisfied, with the parameters $\widetilde{\alpha}_1$ and $\widetilde{\alpha}_2$ expressed as $\widetilde{\alpha}_{1,2} := \frac{1}{2}\Big[1 \pm \alpha\sqrt{3/(1-\alpha^2)}\,\Big]$. Similarly, the exceptional cases are obtained from the arguments in Appendix B.

The above discontinuity angle θ^{cr}, dependent on the stress ratio σ_1/σ_2 and model parameter α, is summarized in Table 2.

Table 2: Discontinuity angles θ^{cr} for the Drucker-Prager criterion in the condition of plane stress

f_c/f_t	Stress ratio σ_1/σ_2										
	-1: -1.24	-1: -2	-1: -5	0: -1	1: -5	1: -1	1: -0.5	1: -0.25	1: -0.15	1: 0	1 : 0.19
2.00	90.00°	51.65°	44.74°	41.81°	39.52°	33.68°	29.90°	26.30°	24.15°	19.47°	0.00°
3.00	43.48°	40.55°	37.35°	35.26°	33.32°	27.37°	22.82°	17.90°	14.51°	0.00°	0.00°
4.00	—	33.66°	32.69°	31.09°	29.33°	23.07°	17.62°	10.53°	0.00°	0.00°	0.00°

With the discontinuity angle (4.32), the traction-based failure criterion can be determined as (see Appendix C for the derivation)

$$t_m^2 - \frac{4\alpha^2-1}{4(1-\alpha^2)}t_n^2 + \frac{\alpha}{1-\alpha}qt_n - \frac{1+\alpha}{3(1-\alpha)}q^2 \le 0 \tag{4.33}$$

As depicted in Fig. 12, the following three cases can be identified for the stress-based failure criterion (4.29) and its projected traction-based counterpart (4.33) regarding the model parameter $\alpha \in [0,1)$ (or, equivalently, $\rho \ge 1$):

- $0 \le \alpha < 1/2$ or $1 \le \rho < 3$: The stress-based failure criterion (4.29) is an ellipse on the $\sigma_1 - \sigma_2$ plane and the traction-based counterpart (4.33) also defines an ellipse on the $t_n - t_m$ plane

  $$t_m^2 + \frac{1-4\alpha^2}{4(1-\alpha^2)}\left[t_n + \frac{2\alpha(1+\alpha)}{1-4\alpha^2}q\right]^2 - \frac{(1+\alpha)^2}{3(1-4\alpha^2)}q^2 \le 0 \tag{4.34}$$

  The classical von Mises criterion belongs to this type (i.e., $\alpha = 0$).

- $\alpha = 1/2$ or $\rho = 3$: The stress-based failure criterion (4.29) defines a parabola on the $\sigma_1 - \sigma_2$ plane, while the traction-based counterpart (4.33) becomes

  $$t_m^2 + qt_n - q^2 \le 0 \tag{4.35}$$

  which is a parabola on the $t_n - t_m$ plane.

- $1/2 < \alpha < 1$ or $\rho > 3$: The stress-based failure criterion (4.29) defines a hyperbola on the $\sigma_1 - \sigma_2$ plane. Similarly, the traction-based counterpart (4.33) is a hyperbola on the $t_n - t_m$ plane, with the left branch of interest given by

  $$\tan\varphi \cdot t_n + \sqrt{t_m^2 + \omega^2 q^2} - c \le 0 \tag{4.36}$$

  where the parameters $\tan\varphi, \omega$ and c are expressed as

  $$\tan\varphi = \sqrt{\frac{4\alpha^2-1}{4(1-\alpha^2)}}, \qquad \omega = \frac{1+\alpha}{\sqrt{3(4\alpha^2-1)}}, \qquad c = \frac{\alpha(1+\alpha)}{\sqrt{(4\alpha^2-1)(1-\alpha^2)}}q \tag{4.37}$$

  This hyperbolic failure criterion asymptotically approaching to a Mohr-Coulomb one has been widely adopted in the modeling of mixed-mode failure in solids [8, 37].

Remark 4.6 For the parameter $\alpha \in [1/2, 1)$, the Drucker-Prager failure criterion (4.29) defines an open surface in the principle $\sigma_1 - \sigma_2$ space. Accordingly, there exists a limit value for the discontinuity angle $\theta^{\rm cr}$. For the parabolic failure criterion (i.e., $\alpha = 1/2$), it follows that

$$\lim_{\sigma_2 \to \sigma_1 < 0} \sin^2 \theta^{\rm cr} = \lim_{\sigma_2 \to \sigma_1 < 0} -\frac{(2\sigma_2 - \sigma_1) + \sqrt{\sigma_1^2 + \sigma_2^2 - \sigma_1\sigma_2}}{3(\sigma_1 - \sigma_2)} = \frac{1}{2} \tag{4.38}$$

Namely, the limit discontinuity angle is $\lim_{\sigma_2 \to \sigma_1 < 0} \theta^{\rm cr} = 45°$. For the hyperbolic one with $\alpha \in (1/2, 1)$, the admissible stress ratio σ_1/σ_2 in the compression-compression quadrant (i.e., $\sigma_1 < 0$ and $\sigma_2 < 0$) is constrained by the parameter α, and so is the discontinuity angle $\theta^{\rm cr}$, i.e.,

$$\sin \theta^{\rm cr} \le \sqrt{\frac{(1 + 2\alpha^2)\sigma_1/\sigma_2 - 2(1 - \alpha^2)}{3(\sigma_1/\sigma_2 - 1)}} \qquad \text{with} \qquad \frac{\sigma_1}{\sigma_2} \le \frac{1 + 2\alpha^2 - \sqrt{3(4\alpha^2 - 1)}}{2(1 - \alpha^2)} \tag{4.39}$$

For instance, it follows that $0° \le \theta^{\rm cr} \le 33.74°$ for the parameter $\rho = 4.0$ (or, equivalently, $\alpha = 0.6$). □

4.6.2. Plane strain

In the case of plane strain, the extra condition (4.4) gives the following out-of-plane stress $\sigma_3 \neq 0$, i.e.,

$$\alpha + \sqrt{\frac{3}{2}} \frac{1}{\|\boldsymbol{s}\|} s_3 = 0 \qquad \Longrightarrow \qquad \sigma_3 = \frac{2\alpha^2 + 1}{2(1 - \alpha^2)}(\sigma_1 + \sigma_2) - \frac{\alpha}{1 - \alpha} q \tag{4.40}$$

As the trace of the deviatoric stress tensor $\boldsymbol{s}$ vanishes, it follows that

$$s_1 + s_2 = -s_3 = \sqrt{\frac{2}{3}}\, \alpha \|\boldsymbol{s}\| \ge 0 \qquad \text{or} \qquad s_1^2 + \frac{6 - 4\alpha^2}{3 - 4\alpha^2}\, s_1 s_2 + s_2^2 = 0 \tag{4.41}$$

Accordingly, the discontinuity angle (4.32) becomes

$$\sin^2 \theta^{\rm cr} = -\frac{s_1 + 2s_2}{s_1 - s_2} = -\frac{\alpha_s + 2}{\alpha_s - 1}, \qquad \cos^2 \theta^{\rm cr} = \frac{2s_1 + s_2}{s_1 - s_2} = \frac{2\alpha_s + 1}{\alpha_s - 1} \tag{4.42}$$

where $\alpha_s := s_1/s_2$ is determined from the relation (4.41)

$$\alpha_s := \frac{s_1}{s_2} = \frac{2\alpha^2 - 3 - 2\alpha\sqrt{3(1 - \alpha^2)}}{3 - 4\alpha^2} \in \big[-1, -2\big] \tag{4.43}$$

The above result holds if the following condition

$$2s_1 + s_2 \ge 0, \qquad s_1 + 2s_2 \le 0 \qquad \Longleftrightarrow \qquad 0 \le \alpha \le \frac{1}{2} \tag{4.44}$$

is satisfied. Compared to the result (4.32) for the case of plane stress, the discontinuity angle $\theta^{\rm cr}$ determined from Eqs. (4.42) and (4.43) depends only on the model parameter $\alpha \in [0, 1/2]$, whatever the stress state is; see Table 3. Note that the result for the von Mises criterion corresponds to the parameter $\alpha = 0$.

Again, the above analytical results, numerically confirmed by Cervera et al. [11], are different from those obtained from the discontinuous bifurcation analysis [53].

Table 3: Discontinuity angles θ^{cr} for the Drucker-Prager criterion in the condition of plane strain

Strength ratio f_c/f_t	1.0	1.50	2.00	2.50	3.00
Discontinuity angle θ^{cr}	45.00°	34.65°	26.12°	17.38°	0.00°

With the above discontinuity angle, the traction-based failure criterion (4.6) can be derived as (see Appendix C)

$$t_m^2 - \frac{3\alpha^2}{1-4\alpha^2}\Big(t_n - \frac{1+\alpha}{3}q\Big)^2 \le 0 \tag{4.45}$$

with the left branch of interest expressed as

$$t_n \cdot \tan\varphi + \big|t_m\big| - c \le 0 \tag{4.46}$$

where the friction angle φ and the cohesion c are given by

$$\tan\varphi = \alpha\sqrt{\frac{3}{1-4\alpha^2}}, \qquad c = \frac{1+\alpha}{\sqrt{3\big(1-4\alpha^2\big)}}q \tag{4.47a}$$

or, equivalently,

$$\alpha = \frac{\tan\varphi}{\sqrt{3+4\tan^2\varphi}}, \qquad \big(1+\alpha\big)q = \frac{3c}{\sqrt{3+4\tan^2\varphi}} \tag{4.47b}$$

That is, in the case of plane strain, the material characterized by the Drucker-Prager model localizes into a Mohr-Coulomb discontinuity. The above relations (4.47) are exactly the matching conditions under which the Drucker-Prager and Mohr-Coulomb models give identical limit load for *perfectly-plastic* materials in the case of plane strain. Upon satisfaction of these plane strain matching conditions, both models produce identical energy dissipation [14].

Remark 4.7 In the case of plane strain, on the one hand, calling for the out-of-plane stress (4.3) the elastic limit surface $\widehat{F}(\boldsymbol{\sigma}, q^0) = 0$ of the Drucker-Prager criterion (4.29) is given by

$$\frac{1}{1+\alpha}\Big[\alpha\big(1+\nu_0\big)\big(\sigma_1+\sigma_2\big) + \sqrt{\big(1-\nu_0+\nu_0^2\big)\big(\sigma_1^2+\sigma_2^2\big) - \big(1+2\nu_0-2\nu_0^2\big)\sigma_1\sigma_2}\Big] = q^0 \tag{4.48}$$

The above elastic limit surface can be either an ellipse for $\alpha < (1/2-\nu_0)/(1+\nu_0)$, a parabola for $\alpha = (1/2-\nu_0)/(1+\nu_0)$, or a hyperbola for $\alpha > (1/2-\nu_0)/(1+\nu_0)$ on the $\sigma_1-\sigma_2$ plane, respectively. On the other hand, for the plane strain localization condition (4.40), the Drucker-Prager criterion (4.29) becomes

$$\big|\sigma_1-\sigma_2\big| = \sqrt{\frac{3}{1-\alpha^2}}\Big[\frac{2}{3}\big(1+\alpha\big)q - \alpha\big(\sigma_1+\sigma_2\big)\Big] \ge 0 \tag{4.49}$$

It follows from Eqs. (4.3) and (4.43) that only for the particular stress state

$$\frac{\sigma_2}{\sigma_1} = \frac{1+\nu_0+\alpha_s\big(2-\nu_0\big)}{2-\nu_0+\alpha_s\big(1+\nu_0\big)} \tag{4.50}$$

can strain localization occur at the onset of softening; see Fig. 13. For all other cases, continuous inelastic deformation and re-orientation of the principal strain directions have to take place until the condition (4.40) or (4.43) is reached, after which strain localization with a strong discontinuity occurs. ■

5. Conclusions

Aiming for the modeling of localized failure in quasi-brittle solids, this paper presents a unified plastic-damage framework based on the framework of irreversible thermodynamics. Both concepts of degradation strain rate and damage strain are incorporated to develop an elastoplastic damage model, with evolution laws for the involved internal variables characterized by a dissipative flow tensor. To explore its use in the modeling of strong or regularized discontinuities, a novel strain localization analysis is proposed to prognosticate the occurrence of strong discontinuities. This is based on continuity of tractions on and across the discontinuity (band), and it results to be more demanding than the classical discontinuous bifurcation condition. The kinematic constraint, on the one hand, is sufficient to guarantee the traction continuity and stress boundedness; on the other hand, it is necessary to reproduce the consistent loading/unloading stress states upon strain localization in softening solids and to guarantee the formation of a fully softened discontinuity.

To have strain localization with a strong (or regularized) discontinuity in softening solids, it is necessary that Maxwell's kinematics of the localized discontinuity (band) be reproduced in an appropriate manner. For the elastoplastic damage model considered in this work, the tensorial components of the dissipative flow tensor in the directions orthogonal to the discontinuity orientation have to vanish upon strain localization. Satisfaction of this kinematic constraint allows developing a localized plastic-damage model for the inelastic discontinuity (band), with both its orientation and the corresponding traction-based failure criterion determined consistently from the given stress-based counterpart. The resulting projected discontinuity approach avoids introducing the cohesive zone model in an *ad hoc* manner. In particular, the involved model parameters can be calibrated from available macroscopic material test data as demonstrated in our previous work [12, 66]. Furthermore, the right instant for the occurrence of strong (or regularized) discontinuities and the introduction of localized models can also be identified.

The aforementioned general results are particularized to 2D conditions of plane stress and plane strain. The discontinuity orientation and the corresponding traction-based failure criterion are obtained in closed-form for a given stress-based counterpart. Finally, the Rankine, Mohr-Coulomb, von Mises (J_2) and Drucker-Prager criteria are analyzed as illustrative examples, with the analytical discontinuity angles coincident with those results obtained from numerical simulations. It is found that in the case of plane stress, strain localization with stress boundedness/continuity can occur at the onset of strain softening. Contrariwise, owing to the extra kinematic constraint, in the condition of plane strain some continuous inelastic deformations and substantial re-orientation of principal strain directions have to take place first prior to strain localization.

6. Acknowledgments

Support from the National Natural Science Foundation of China (51222811, 51008130) and the State Key Laboratory of Subtropical Building Science (2015ZB24) to the first author (J.Y. Wu) is acknowledged. Support from the

Spanish Ministry of Economy and Competitivity under the project Enhanced Accuracy Computational Framework for Strain Localization and Failure Mechanisms (EACY) – is acknowledged by the second author (M. Cervera).

Appendix A. Mohr's maximization postulate

Mohr's maximization postulate Mohr [35] assumes that a discontinuity (band) is initiated on the orientation $\boldsymbol{n}(\widehat{\boldsymbol{\theta}}^{\mathrm{cr}})$ upon which the tractions maximize the failure function $\widehat{f}\big[\boldsymbol{t}(\boldsymbol{\theta}), q\big]$, i.e.,

$$\widehat{\boldsymbol{\theta}}^{\mathrm{cr}} = \arg\max \widehat{f}\big[\boldsymbol{t}(\boldsymbol{\theta}), q\big] = \arg\max \widehat{f}\big[\boldsymbol{\sigma}\cdot\boldsymbol{n}(\boldsymbol{\theta}), q\big] \tag{A.1}$$

with $\widehat{\boldsymbol{\theta}}^{\mathrm{cr}}$ being the characteristic angles. Mathematically, the following stationarity condition holds

$$\left.\frac{\partial \widehat{f}}{\partial \boldsymbol{\theta}}\right|_{\widehat{\boldsymbol{\theta}}^{\mathrm{cr}}} = \left(\widehat{\boldsymbol{\gamma}}\cdot\frac{\partial \boldsymbol{t}}{\partial \boldsymbol{\theta}}\right)_{\widehat{\boldsymbol{\theta}}^{\mathrm{cr}}} = \left(\widehat{\gamma}_n\frac{\partial t_n}{\partial \boldsymbol{\theta}} + \widehat{\gamma}_m\frac{\partial t_m}{\partial \boldsymbol{\theta}} + \widehat{\gamma}_p\frac{\partial t_p}{\partial \boldsymbol{\theta}}\right)_{\widehat{\boldsymbol{\theta}}^{\mathrm{cr}}} = \boldsymbol{0} \tag{A.2}$$

together with a negative-definite Hessian matrix $\partial^2\widehat{f}/\partial\boldsymbol{\theta}^2$ at the discontinuity angles $\widehat{\boldsymbol{\theta}}^{\mathrm{cr}}$.

Calling for the identity $\boldsymbol{\Lambda} : (\partial\boldsymbol{\sigma}/\partial\boldsymbol{\theta}) = 0$ resulting from the coaxial property between the tensors $\boldsymbol{\Lambda} := \partial\widehat{f}/\partial\boldsymbol{\sigma}$ and $\boldsymbol{\sigma}$ [29], it follows from the relations (3.18) and (A.2) that [66]

$$\left.\frac{\partial \widehat{f}}{\partial \boldsymbol{\theta}}\right|_{\widehat{\boldsymbol{\theta}}^{\mathrm{cr}}} = -\left(\Lambda_{mm}\frac{\partial\sigma_{mm}}{\partial\boldsymbol{\theta}} + 2\Lambda_{mp}\frac{\partial\sigma_{mp}}{\partial\boldsymbol{\theta}} + \Lambda_{pp}\frac{\partial\sigma_{pp}}{\partial\boldsymbol{\theta}}\right)_{\widehat{\boldsymbol{\theta}}^{\mathrm{cr}}} = \boldsymbol{0} \tag{A.3}$$

As the failure function $\widehat{f}(\boldsymbol{t}, q) \leq 0$ depends only on the tractions $\boldsymbol{t} := \{\sigma_{nn}, \sigma_{nm}, \sigma_{np}\}^{\mathrm{T}}$, the condition (A.3) is fulfilled for arbitrary values of the remaining stress components $(\sigma_{mm}, \sigma_{mp}, \sigma_{pp})$. This fact yields

$$\Lambda_{mm}(\widehat{\boldsymbol{\theta}}^{\mathrm{cr}}) = 0, \qquad \Lambda_{pp}(\widehat{\boldsymbol{\theta}}^{\mathrm{cr}}) = 0, \qquad \Lambda_{mp}(\widehat{\boldsymbol{\theta}}^{\mathrm{cr}}) = 0 \tag{A.4}$$

The above relations correspond exactly to the kinematic constraints (3.19).

If the solution to Eqs. (A.4) does not exist, the discontinuity angles $\widehat{\boldsymbol{\theta}}^{\mathrm{cr}}$ should be determined from another set of solution to Eqs. (A.3)

$$\left.\frac{\partial\sigma_{mm}}{\partial\boldsymbol{\theta}}\right|_{\widehat{\boldsymbol{\theta}}^{\mathrm{cr}}} = 0, \qquad \left.\frac{\partial\sigma_{mp}}{\partial\boldsymbol{\theta}}\right|_{\widehat{\boldsymbol{\theta}}^{\mathrm{cr}}} = 0, \qquad \left.\frac{\partial\sigma_{pp}}{\partial\boldsymbol{\theta}}\right|_{\widehat{\boldsymbol{\theta}}^{\mathrm{cr}}} = 0 \tag{A.5}$$

Contrariwise, for the stress-based projected discontinuity model, if the solution to the kinematic constraints (3.19) does not exist, strain localization into a strong (regularized) discontinuity cannot occur. In this exceptional situation, for both families of approaches to be completely equivalent as shown in Wu and Cervera [65, 66], the given stress-based failure criterion can be modified based on the solution to Eq. (A.5); see Appendix B for the 2D cases.

Appendix B. Exceptional 2D cases

For 2D cases in which $\widehat{\Lambda}_2 > 0$ or $\widehat{\Lambda}_1 < 0$, the discontinuity angle determined from Eq. (4.2) does not hold. It implies that strain localization into a strong (regularized) discontinuity cannot occur for the given stress-based failure criterion $\widehat{F}(\boldsymbol{\sigma}, q) \leq 0$.

In this exceptional situation, some necessary modification should be made in such a way that strain localization into a strong (regularized) discontinuity may still occur and the resulting projected discontinuity approach is completely equivalent to the strong/regularized ones. That is, the discontinuity angle is given from the solution to Eqs. (A.5), or more specifically, the maximization conditions (4.7) and (4.8), i.e.,

$$\sin(2\theta^{\mathrm{cr}}) = 0 \qquad \Longrightarrow \qquad \theta^{\mathrm{cr}} = \begin{cases} 0 & \widehat{\Lambda}_1 > \widehat{\Lambda}_2 > 0 \\ \pi/2 & \widehat{\Lambda}_2 < \widehat{\Lambda}_1 < 0 \end{cases} \tag{B.1}$$

which corresponds to the limit values $\widehat{\Lambda}_2 = 0$ and $\widehat{\Lambda}_1 = 0$ in the general case (4.2), respectively.

Accordingly, the given stress-based failure function $\widehat{F}(\boldsymbol{\sigma}, q)$ is modified as

$$\widehat{F}(\boldsymbol{\sigma}, q) = \begin{cases} \dfrac{1}{M}\Big[\Big(\widehat{\Lambda}_1\Big|_{\widehat{\Lambda}_2=0}\Big)\sigma_1 - \widehat{h}\cdot q\Big] & \widehat{\Lambda}_1 > \widehat{\Lambda}_2 > 0 \\ \dfrac{1}{M}\Big[\Big(\widehat{\Lambda}_2\Big|_{\widehat{\Lambda}_1=0}\Big)\sigma_2 - \widehat{h}\cdot q\Big] & \widehat{\Lambda}_2 < \widehat{\Lambda}_1 < 0 \end{cases} \tag{B.2}$$

As depicted in Figs. 10(a) and 12, this modification introduces tension- and compression-extensions into the original stress-based failure criterion $\widehat{F}(\boldsymbol{\sigma}, q) \leq 0$. Similarly, the projected traction-based failure function $f(\boldsymbol{t}, q)$ is given by

$$f(\boldsymbol{t}, q) = \begin{cases} \dfrac{1}{M}\Big[\Big(\widehat{\Lambda}_1|_{\widehat{\Lambda}_2=0}\Big)t_n - \widehat{h}\cdot q\Big] & \widehat{\Lambda}_1 > \widehat{\Lambda}_2 > 0 \\ \dfrac{1}{M}\Big[\Big(\widehat{\Lambda}_2|_{\widehat{\Lambda}_1=0}\Big)t_n - \widehat{h}\cdot q\Big] & \widehat{\Lambda}_2 < \widehat{\Lambda}_2 < 0 \end{cases} \tag{B.3}$$

where the tangential traction is removed from the failure criterion (4.6). With the above modifications, the stress- and traction-based models are completely equivalent to each other as shown in Wu and Cervera [65, 66].

Appendix C. Traction-based failure criteria for the Drucker-Prager model

In the case of plane stress, for the discontinuity angle (4.32) it follows that

$$t_n = \frac{2}{3}\Big[\alpha(1+\alpha)q + (1-\alpha^2)(\sigma_1+\sigma_2)\Big] \tag{C.1a}$$

$$t_m^2 = -\Big(\sqrt{2/3}\,\alpha\|\boldsymbol{s}\| + s_1\Big)\Big(\sqrt{2/3}\,\alpha\|\boldsymbol{s}\| + s_2\Big) \tag{C.1b}$$

Accordingly, the normal and tangential components (γ_n, γ_m) in Eq. (4.5) become

$$\gamma_n = \frac{1}{(1+\alpha)\sqrt{2/3}\,\|\boldsymbol{s}\|}\,\frac{(1-4\alpha^2)t_n + 2\alpha(1+\alpha)q}{2(1-\alpha^2)} \tag{C.2a}$$

$$\gamma_m = \frac{1}{(1+\alpha)\sqrt{2/3}\,\|\boldsymbol{s}\|}\,2t_m \tag{C.2b}$$

where the norm $\|\boldsymbol{s}\|$ is evaluated from Eq. (4.31) as

$$\sqrt{\frac{2}{3}}\,\|\boldsymbol{s}\| = \frac{1}{1-\alpha^2}\Big[\frac{2}{3}(1+\alpha)q - \alpha t_n\Big] \geq 0 \tag{C.3}$$

Therefore, the definition (4.6) gives the following traction-based failure function

$$\frac{2}{(1+\alpha)\sqrt{2/3}\,\|\boldsymbol{s}\|}\left[t_m^2-\frac{4\alpha^2-1}{4(1-\alpha^2)}t_n^2+\frac{\alpha}{1-\alpha}qt_n-\frac{1+\alpha}{3(1-\alpha)}q^2\right]\le 0 \tag{C.4}$$

which can be transformed into the homogeneous failure function (4.33) of degree $M=2$.

In the case of plane strain, the discontinuity angle (4.42) leads to the following normal traction t_n

$$t_n=\sigma_1+\sigma_2-\sigma_3=\frac{(1-4\alpha^2)(\sigma_1+\sigma_2)+2\alpha(1+\alpha)q}{2(1-\alpha^2)} \tag{C.5}$$

which yields the following relations

$$\sigma_1+\sigma_2=\frac{2(1-\alpha^2)t_n-2\alpha(1+\alpha)q}{1-4\alpha^2} \tag{C.6a}$$

$$\sigma_3=\frac{(1+2\alpha^2)t_n-2\alpha(1+\alpha)q}{1-4\alpha^2} \tag{C.6b}$$

Similarly, the square of the tangential traction t_m^2 is given by

$$t_m^2=-(2s_1+s_2)(s_1+2s_2) \tag{C.7}$$

Accordingly, the normal and tangential components (γ_n,γ_m) are evaluated from Eq. (4.5) as

$$\gamma_n=\frac{3\alpha}{1+\alpha},\qquad \gamma_m=\frac{2\alpha}{1+\alpha}\cdot\frac{t_m}{s_1+s_2} \tag{C.8}$$

where the following relation applies

$$s_1+s_2=\frac{\sigma_1+\sigma_2-2\sigma_3}{3}=\frac{2\alpha}{3(1-4\alpha^2)}\Big[-3\alpha t_n+(1+\alpha)q\Big]\ge 0 \tag{C.9}$$

owing to the relation (4.41). It then follows from Eq. (4.6) that

$$f(\boldsymbol{t},q)=\frac{1}{1+\alpha}\left[\frac{3(1-4\alpha^2)}{(1+\alpha)q-3\alpha t_n}t_m^2-3\alpha t_n+(1+\alpha)q\right]\le 0 \tag{C.10}$$

which can be transformed into the form (4.45).

References

[1] Abu Al-Rub, R.K. and Darabi, M.K., 2012. A thermodynamic framework for constitutive modeling of time- and rate-dependent materials. Part I: Theory. *Int. J. Plast.*, 34: 61-92.

[2] Armero, F., 1999. Large-scale modeling of localized dissipative mechanisms in a local continuum: applications to the numerical simulation of strain localization in rate-dependent inelastic solids. *Mech. Cohes.-Frict. Mater.*, 4: 101-131.

[3] Armero, F. and Oller, S., 2000. A general framework for continuum damage models. I: Infinitesimal plastic damage models in stress space. *Int. J. Solids Structures*, 37: 7409-7464.

[4] Armero, F. and Kim, J., 2012. Three-dimensional finite elements with embedded strong discontinuities to model material failure in the infinitesimal range. *Int. J. Numer. Meth. Engng*, 91: 1291-1330.

[5] Barenblatt, G.I., 1959. The formation of equilibrium cracks during brittle fracture. General ideas and hypotheses. Axially-symmetric cracks. *J. Applied Mathematics and Mechanics*, 23: 622-636.

[6] Besson, J., Steglich, D. and Brocks, W., 2003. Modeling of plane strain ductile rupture. *Int. J. Plast.*, 19: 1517-1541.

[7] Bažant, Z.P. and Oh, B.H., 1983. Crack band theory for fracture of concrete. Materials and Structures (RILEM, Paris), 16: 155–177.

[8] Carol, I., Prat, P., and López, C., 1997. Normal/shear cracking model: Application to discrete crack analysis. *J. Eng. Mech., ASCE*, 123(8): 765-773.

[9] Carol, I., Rizzi, E., Willam, K., 1994. A unified theory of elastic degradation and damage based on a loading surface. *Int. J. Solids Structures*, 31(20): 2835-2865.

[10] Cervera, M., Chiumenti, M. and Di Capua, D., 2012. Benchmarking on bifurcation and localization in J_2 plasticity for plane stress and plane strain conditions. *Comput. Methods Appl. Mech. Engrg.*, 241-244: 206-224.

[11] Cervera, M., Chiumenti, M. Benedetti, L. and Codina, R., 2015. Mixed stabilized finite element methods in nonlinear solid mechanics. Part III: Compressible and incompressible plasticity. *Comput. Methods Appl. Mech. Engrg.*, 285: 752-775.

[12] Cervera, M. and Wu, J.Y., 2015. On the conformity of strong, regularized, embedded and smeared discontinuity approaches for the modeling of localized failure in solids. *Int. J. Solids Structures*, http://dx.doi.org/10.1016/j.ijsolstr.2015.05.016. Colorado, Boulder.

[13] Chaboche, J.L., 2008. A review of some plasticity and viscoplasticity constitutive theories. *Int. J. Plast.*, 24: 1642-1693.

[14] Chen, W.F., 1994. Constitutive Equations for Engineering Materials: Plasticity and Modeling, vol. 2. Elsevier, Amsterdam.

[15] Dugdale, D., 1960. Yielding of steel sheets containing slits. *J. Mech. Phys. Solids*, 8: 100-108.

[16] Dumstorff, P. and Meschke, G., 2006. Crack propagation criteria in the framework of X-FEM-based structural analysis. *Int. J. Numer. Anal. Meth. Geomech*, 31: 239-259.

[17] Dequiedt, J.L., 2013. Localization in heterogeneous materials: A variational approach and its application to polycrystalline solids. *Int. J. Plast.*, 48: 92-110.

[18] Franz, G., et al., 2009. Ellipticity loss analysis for tangent moduli deduced from a large strain elasticplastic self-consistent model. *Int. J. Plast.*, 25: 205-238.

[19] Franz, G., Abed-Meraim, F. and Berveiller, M., 2013. Strain localization analysis for single crystals and polycrystals: Towards microstructure-ductility linkage. *Int. J. Plast.*, 48: 1-33.

[20] Golub, G.H. and van Loan, C.F., 1996. Matrix computations, third edition (page 50). The John Hopkins University Press, Baltimore.

[21] Haddag, B., Abed-Meraim, F. and Balan, T., 2009. Strain localization analysis using a large deformation anisotropic elastic-plastic model coupled with damage. *Int. J. Plast.*, 25: 1970-1996.

[22] Hansbo, A. and Hansbo, P., 2004. A finite element method for the simulation of strong and weak discontinuities in solid mechanics. *Comput. Methods Appl. Mech. Engrg.*, 193: 3523-3540.

[23] Hill, R., 1958. General theory of uniqueness and stability of elasto-plastic solids. *J. Mech. Phys. Solids*, 6: 236–249.

[24] Hill, R., 1962. Acceleration waves in solids. *J. Mech. Phys. Solids*, 10: 1–16.

[25] Hillerborg, A., Modeer, M. and Petersson, P.E., 1976. Analysis of crack formation and crack growth in concrete by means of fracture mechanics and finite elements. *Cement Concrete Res.*, 6: 773-782.

[26] Horstemeyer, M.F. and Bammann, D.J., 2010. Historical review of internal state variable theory for inelasticity. *Int. J. Plast.*, 26: 1310-1334.

[27] Huespe, A.E., Needleman, A., Oliver, J. and Sánchez, P.J., 2009. A finite thickness band method for ductile fracture analysis. *Int. J. Plast.*, 25: 2349-2365.

[28] Huespe, A.E., Needleman, A., Oliver, J. and Sánchez, P.J., 2012. A finite strain, finite band method for modeling ductile fracture. *Int. J. Plast.*, 28: 53-69.

[29] Itskov, M., 2007. *Tensor algebra and tensor analysis for engineers: With applications to continuum mechanics*. Springer, Berlin.

[30] Jirásek, M. and Zimmermann, T., 2001. Embedded crack model. Part II: Combination with smeared cracks. *Internat. J. Numer. Methods Engrg.*, 50(6): 1291-1305.

[31] Jirásek, M. and Rolshoven, S., 2009. Localization properties of strain-softening gradient plasticity models. Part I: strain-gradient theories. *Int. J. Solids Struct.*, 46(11-12): 2225-2238.

[32] Krajcinovic, D., 2003. Damage Mechanics. Elsevier B.V., Netherlands.

[33] Lubarda, V.A., 2002. *Elastoplasticity Theory*. CRC Press, New York.

[34] Meschke, G, Lackner, R. and Mang, H.A., 1998. An anisotropic elastoplastic damage model for plain concrete. *Int. J. Numer. Meth. Engng.*, 42: 703-727.

[35] Mohr, O., 1900. Welche Umstände bedingen die Elastizitätsgrenze und den Bruch eines Materials? *Civilingenieur: Zeitschrift des Vereins deutscher Ingenieure*, VDI 44/45: 1524-1530; 1572-1577.

[36] Mosler, J., 2005. On advanced solution strategies to overcome locking effects in strong discontinuity approaches. *Int. J. Numer. Methods Eng.*, 63, 1313-1341.

[37] Most, T. and Bucher, C., 2007. Energy-based simulation of concrete cracking using an improved mixed-mode cohesive crack model within a meshless discretization. *Int. J. Numer. Anal. Meth. Geomech.*, 31: 285-305

[38] Ngo, D., Scordelis, A.C., 1967. Finite element analysis of reinforced concrete beams, *ACI J.*, 64(14): 152-163.

[39] Oliver, J., 1996. Modeling strong discontinuities in solid mechanics via strain softening contitutive equations. Part I: Fundaments & Part II: Numerical simulation. *Int. J. Numer. Meth. Engng*, 39: 3575-3623.

[40] Oliver, J., Cervera, M. and Manzoli, O. 1998. On the use of strain-softening models for the simulation of strong discontinuities in solids. *Material instabilities in solids*: 107-123, Wiley.

[41] Oliver, J. Cervera, M. and Manzoli, O., 1999. Strong discontinuities and continuum plasticity models: the strong discontinuity approach. *Int. J. Plast.*, 15: 319-351.

[42] Oliver, J., 2000. On the discrete constitutive models induced by strong discontinuity kinematics and continuum constitutive equations. *Int. J. Solids Structures*, 37: 7207-7229.

[43] Oliver, J., Huespe, A.E., Pulido, M.D.G., Chaves, E., 2002. From continuum mechanics to fracture mechanics: the strong discontinuity approach. *Eng. Fract. Mech.*, 69: 113-136.

[44] Oliver, J., Huespe, A.E. and Sànchez, P.J., 2006. A comparative study on finite elements for capturing strong discontinuities: E-FEM vs X-FEM. *Comput. Methods Appl. Mech. Engrg.*, 195: 4732-4752.

[45] Oliver, J., Huespe, A.E., Pulido, M.D.G., Blanco, S. and Linero, D., 2006. On the fracture models determined by the continuum-strong discontinuity approach. *Int. J. Fract.*, 137: 211-229.

[46] Oliver, J., Huespe, A.E. and Dias, I.F., 2012. Strain localization, strong discontinuities and material fracture: Matches and mismatches. *Comput. Methods Appl. Mech. Engrg.*, 241-244: 323-336.

[47] Ortiz., M., 1985. A constitutive theory for the inelastic behavior of concrete. *Mech. Mater.*, 4: 76-93.

[48] Rashid, Y., 1968. Analysis of prestressed concrete pressure vessels. *Nucl. Eng. Des.*, 7: 334-344.

[49] Remmers, J.J.C., de Borst, R., Verhoosel, C.V. and Needleman, A., 2013. The cohesive band model: a cohesive surface formulation with stress triaxiality. *Int. J. Fract.*, 181: 177-188.

[50] Rice, J.R. and Rudnicki, J.W., 1980. A note on some features of the theory of localization of deformation. *Int. J. Solids Structures*, 16: 597-605.

[51] Rots, J.G., 1988. Computational modeling of concrete fracture. *Doctoral Dissertation*, Delft University of Technology, Delft, The Netherlands.

[52] Rudnicki, J.W. and Rice, J.R., 1975. Conditions of the localization of deformation in pressure-sensitive dilatant material. *J. Mech. Phys. Solids*, 23: 371–394.

[53] Runesson, K., Ottosen, N.S. and Peric, D., 1991. Discontinuous bifurcations of elastic-plastic solutions at plane stress and plane strain. *Int. J. Plast.*, 7: 99-121.

[54] Sánchez, P.J., Huespe, A.E. and Oliver, J., 2008. On some topics for the numerical simulation of ductile fracture. *Int. J. Plast.*, 24: 1008-1038.

[55] Svedberg, T. and Runesson, K., 1997. A thermodynamically consistent theory of gradient-regularized plasticity coupled to damage. *Int. J. Plast.*, 13: 669-696.

[56] Simó, J.C., Oliver, J. and Armero, F., 1993. An analysis of strong discontinuities induced by strain-softening in rate-independent inelastic solids. *Comput. Mech.* , 12: 277-296.

[57] Thomas, T.Y., 1961. *Plastic Flow and Fracture of Solids*. Academic Press, New York.

[58] Voyiadjis, G.Z., Alsaleh, M.I. and Alshibli, K.A., 2005. Evolving internal length scales in plastic strain localization for granular materials. *Int. J. Plast.*, 21: 2000-2024.

[59] Voyiadjis, G.Z., Dorgan, R.J., 2007. Framework using functional forms of hardening internal state variables in modeling elasto-plastic-damage behavior. *Int. J. Plast.*, 23: 1826-1859.

[60] Vrech, S., Etse, G., 2005. Geometrical localization analysis of gradient-dependent parabolic Drucker-Prager elastoplasticity. *Int. J. Plast.*, 22(5): 943-964.

[61] Wells, G.N. and Sluys, L.J., 2001. A new method for modelling cohesive cracks using finite elements. *Int. J. Numer. Meth.*

Engng., 50: 2667-2682.

[62] Wu, J. Y., 2011. Unified analysis of enriched finite elements for modeling cohesive cracks. *Comput. Methods Appl. Mech. Engrg.*, 200(45-46): 3031-3050.

[63] Wu, J. Y., Cervera, M., 2013. Strain localization in elastoplastic damage solids. In: *Proceedings of International Symposium on Innovation & Sustainability of Structures in Civil Engineering (ISISS-2013)*, Harbin, China.

[64] Wu, J. Y., Cervera, M., 2014a. On the stress continuity condition for strain localization in softening solids. In: *Proceedings of 11th World Congress On Computational Mechanics (WCCM-2014)*, Barcelona, Spain.

[65] Wu, J. Y., Cervera, M., 2014b. Strain localization and failure mechanics for elastoplastic damage solids. *Monograph CIMNE*, M147, Barcelona, Spain.

[66] Wu, J. Y., Cervera, M., 2015. On the equivalence between traction- and stress-based approached for the modeling of localized failure in solids. *J. Mech. Phys. Solids*, 82: 137-163.

[67] Wu, J.Y. and Xu, S.L., 2011. An augmented multicrack elastoplastic damage model for tensile cracking. *Int. J. Solids Structures*, 48: 2511-2528.

[68] Wu, J.Y. and Xu, S.L., 2013. Reconsideration on the elastic damage/degradation theory for the modeling of microcrack closure-reopening (MCR) effects. *Int. J. Solids Structures*, 50(5): 795-805.

[69] Wu, J.Y., Li, J. and Faria, R., 2006. An energy release rate-based plastic-damage model for concrete. *Int. J. Solids Structures*, 43(3-4): 583-612.

[70] Wu, J. Y., Li, F. B. and Xu, S. L., 2015. Extended embedded finite elements with continuous displacement jumps for the modeling of localized failure in solids. *Comput. Methods Appl. Mech. Engrg.*, 285: 346-378.

[71] Wu, J. Y. and Li, F. B., 2015. An improved stable XFEM (Is-XFEM) with a novel enrichment function for the computational modeling of cohesive cracks. *Comput. Methods Appl. Mech. Engrg.*, http://dx.doi.org/10.1016/j.cma.2015.06.018.

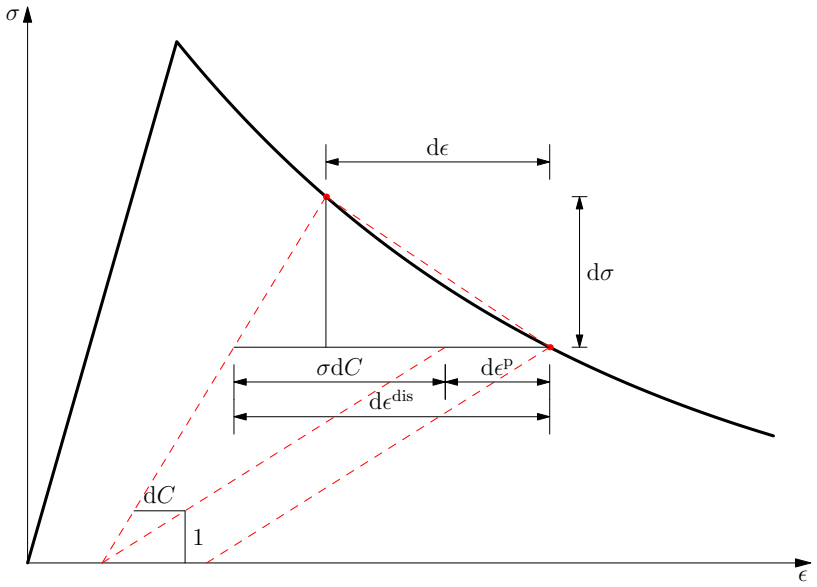

Figure 1: 1-D definition of the dissipative strain tensor and its damage/plastic components

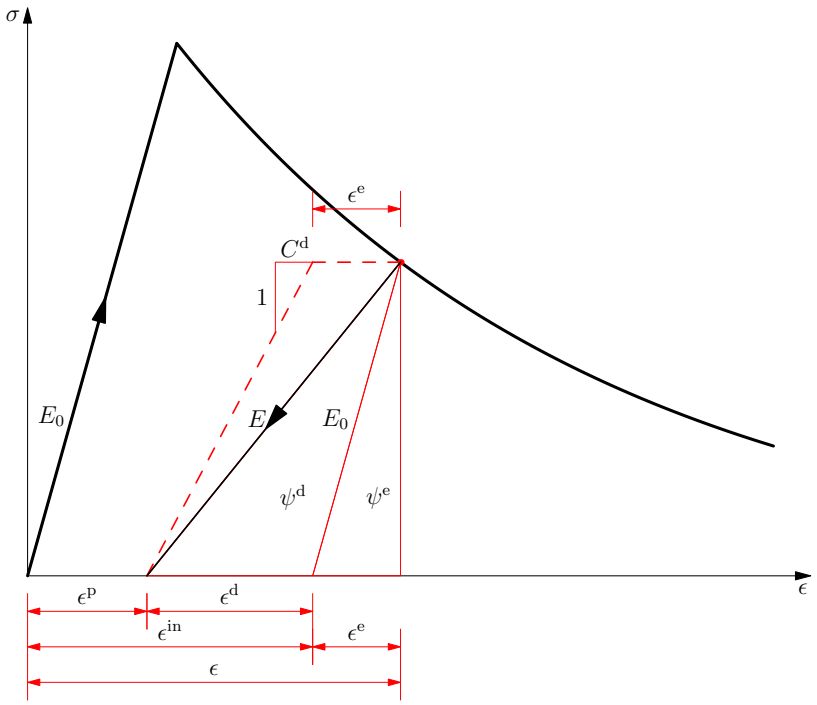

Figure 2: Different kinematic decompositions adopted in the unified elastoplastic damage model

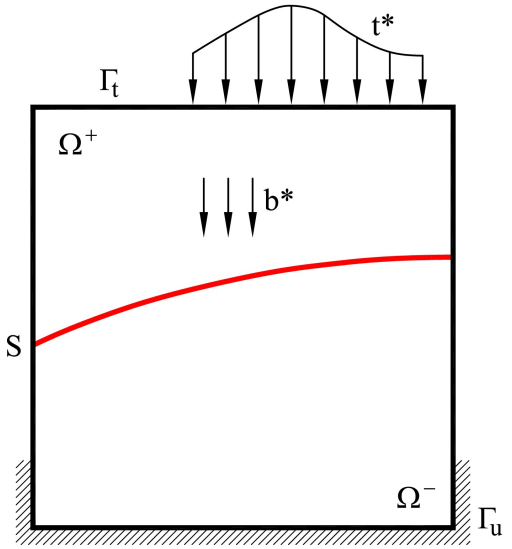

Figure 3: Problem setting in an elastic solid medium with an internal discontinuity

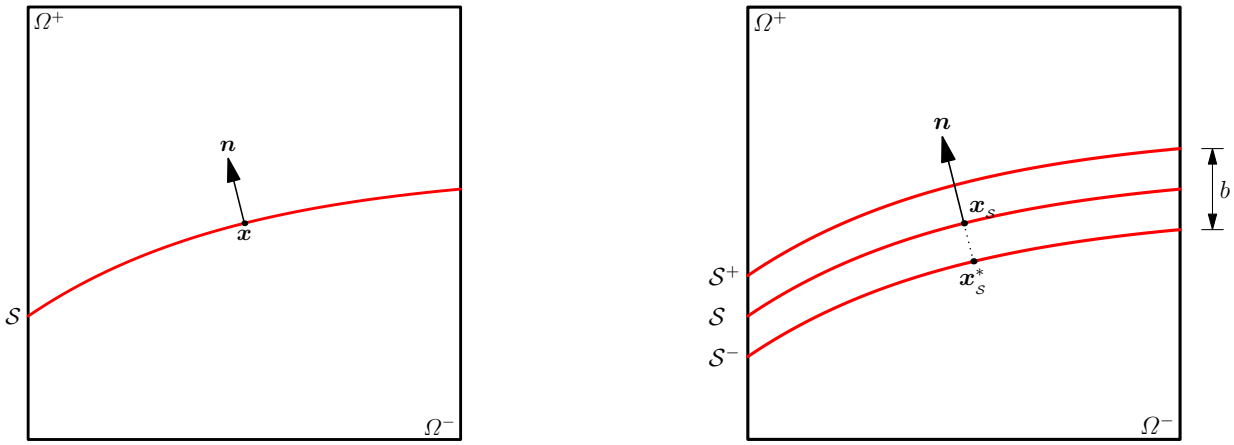

(a) Strong discontinuity

(b) Regularized discontinuity

Figure 4: Strong and regularized discontinuities in a solid

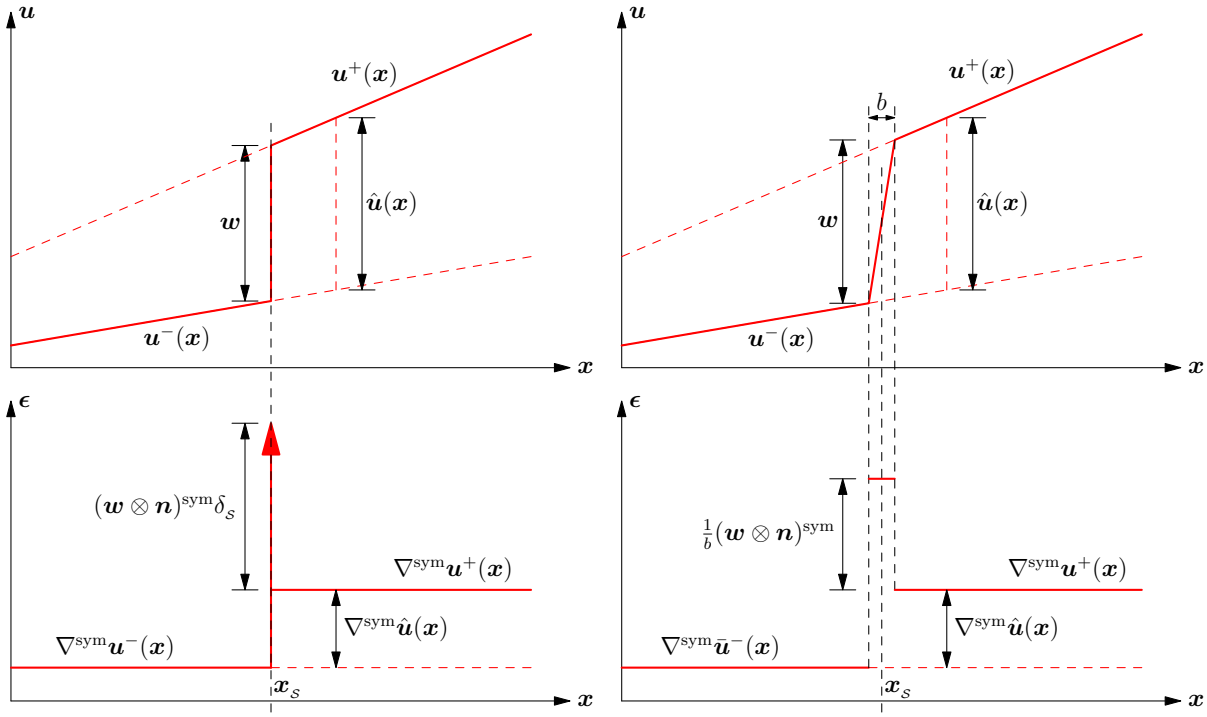

(a) Displacement/strain fields around a strong discontinuity (b) Displacement/strain fields around a regularized discontinuity

Figure 5: Kinematics of strong/regularized discontinuities

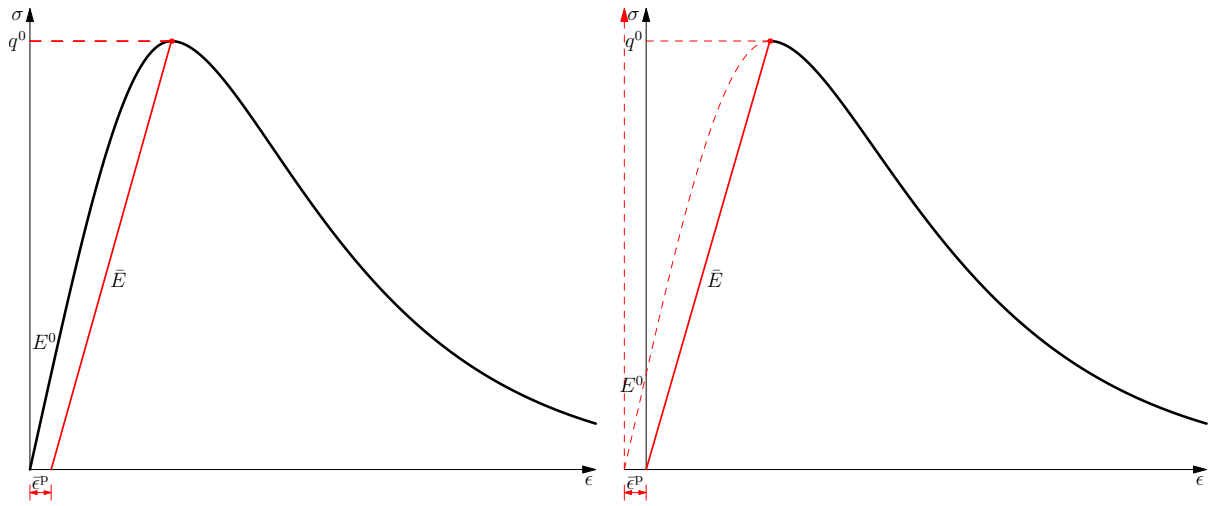

(a) Continuous deformations prior to strain localization (b) Discontinuous deformations post strain localization

Figure 6: Nonlinear behavior caused by continuous deformations prior to strain localization and the equivalent linear elastic bulk material

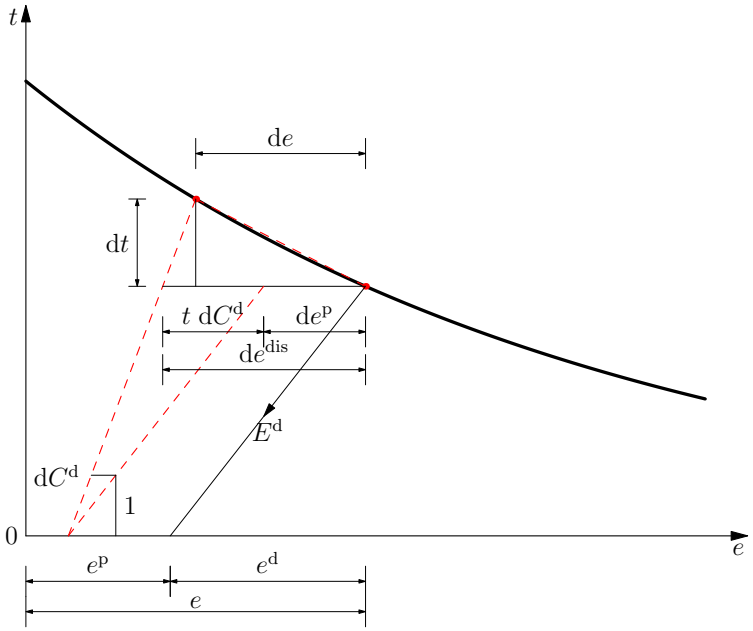

Figure 7: 1-D definition of the dissipative deformation vector rate and its damage/plastic components

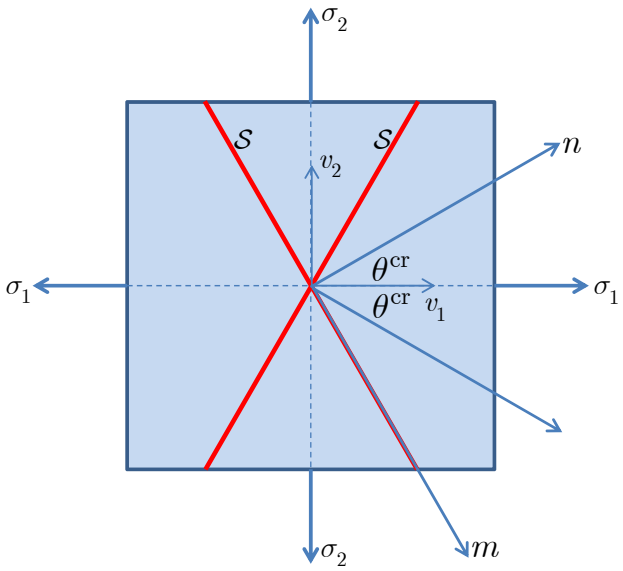

Figure 8: Definition of the discontinuity angle

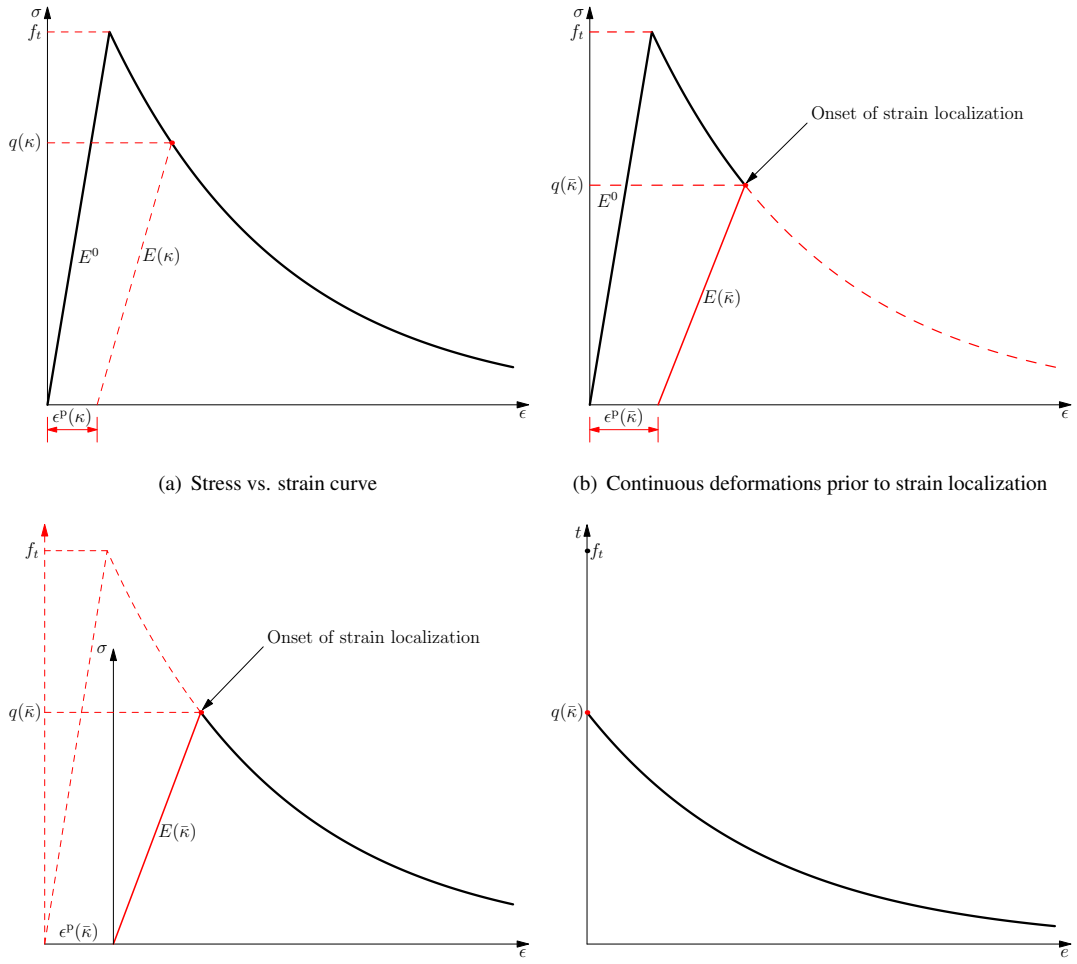

(a) Stress vs. strain curve

(b) Continuous deformations prior to strain localization

(c) Discontinuous deformations post strain localization

(d) Traction vs. *localized* inelastic deformation vector

Figure 9: Delayed strain localization in the condition of plane strain. Here, κ denotes the strain-like internal variable, and $\bar{\kappa}$ represents the corresponding value at the onset of strain localization.

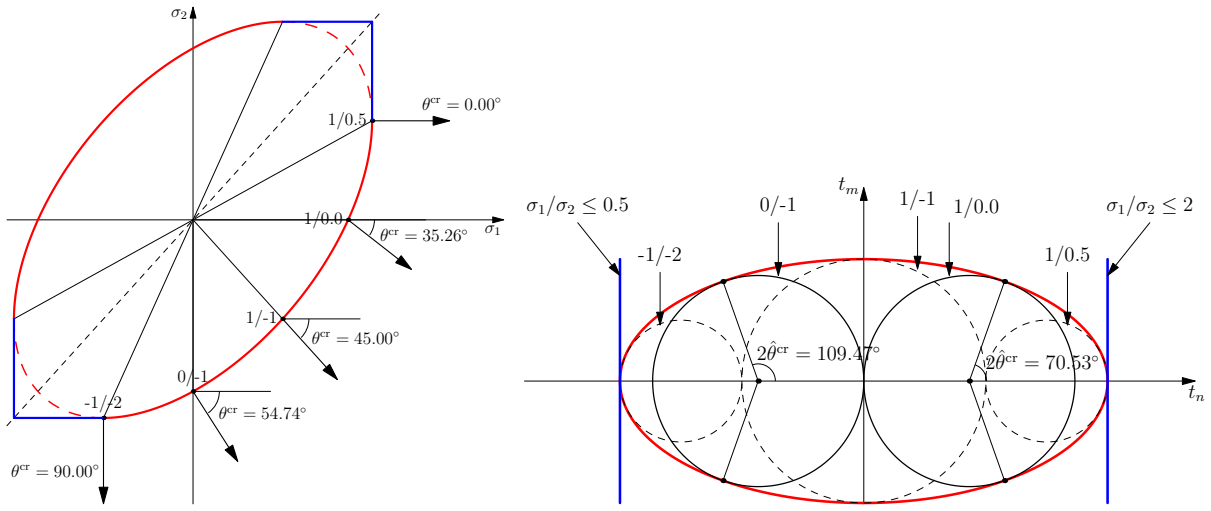

(a) Principal stress space

(b) Traction space

Figure 10: Discontinuity angles of the von Miese criterion in the condition of plane stress

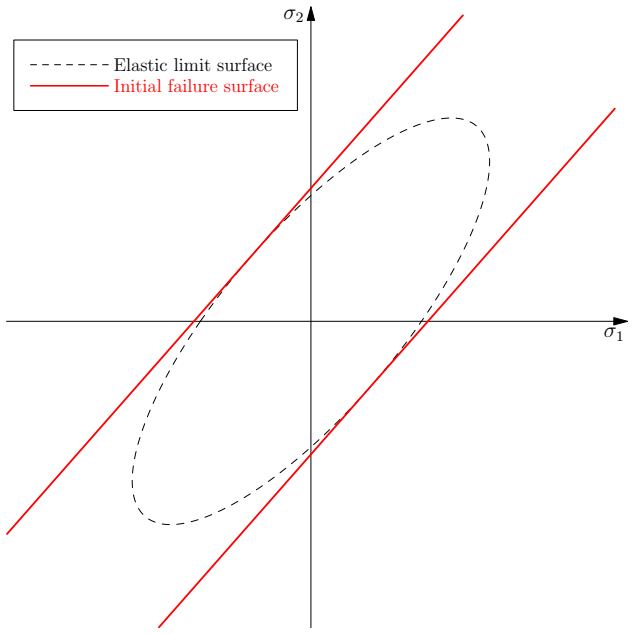

Figure 11: Elastic limit surface and initial failure surface of the von Miese criterion in the condition of plane strain

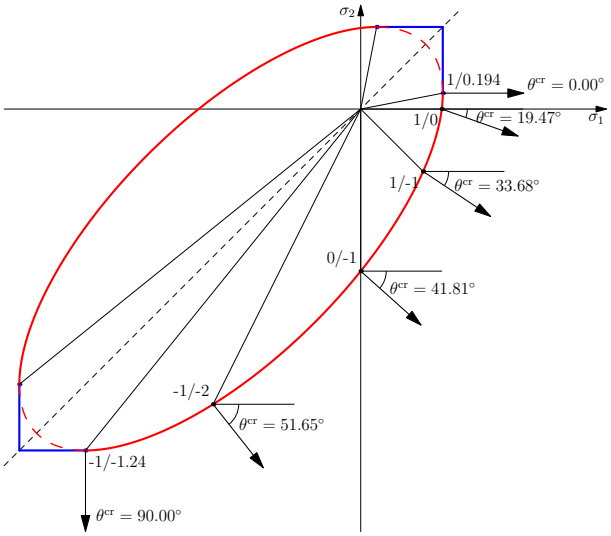

(a) Elliptic type ($\rho = 2.0$)

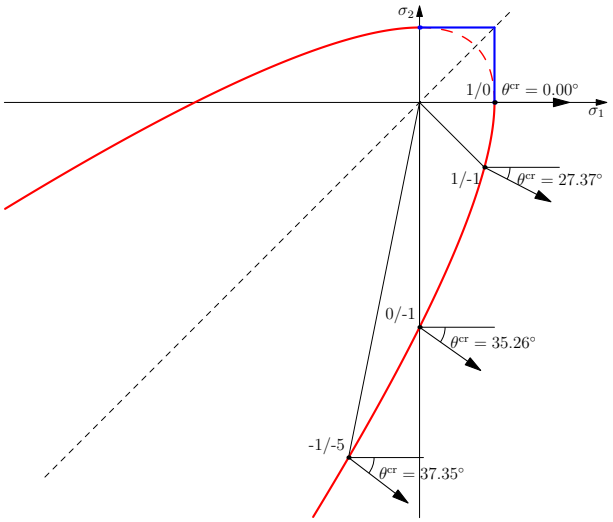

(b) Parabolic type ($\rho = 3.0$)

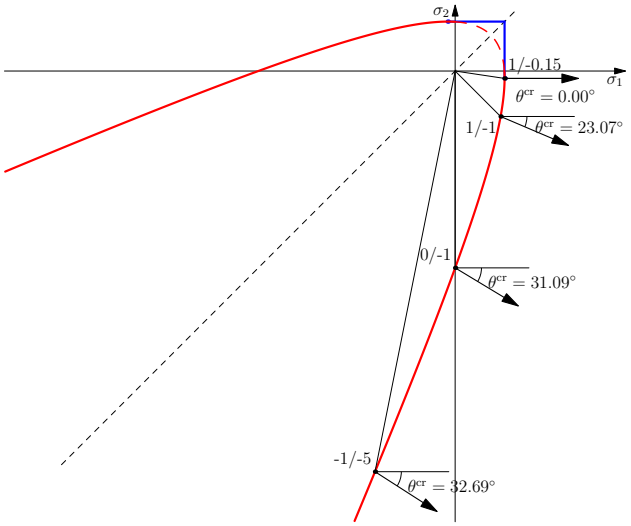

(c) Hyperbolic type ($\rho = 4.0$)

Figure 12: The Drucker-Prager criteria of different types in the condition of plane stress

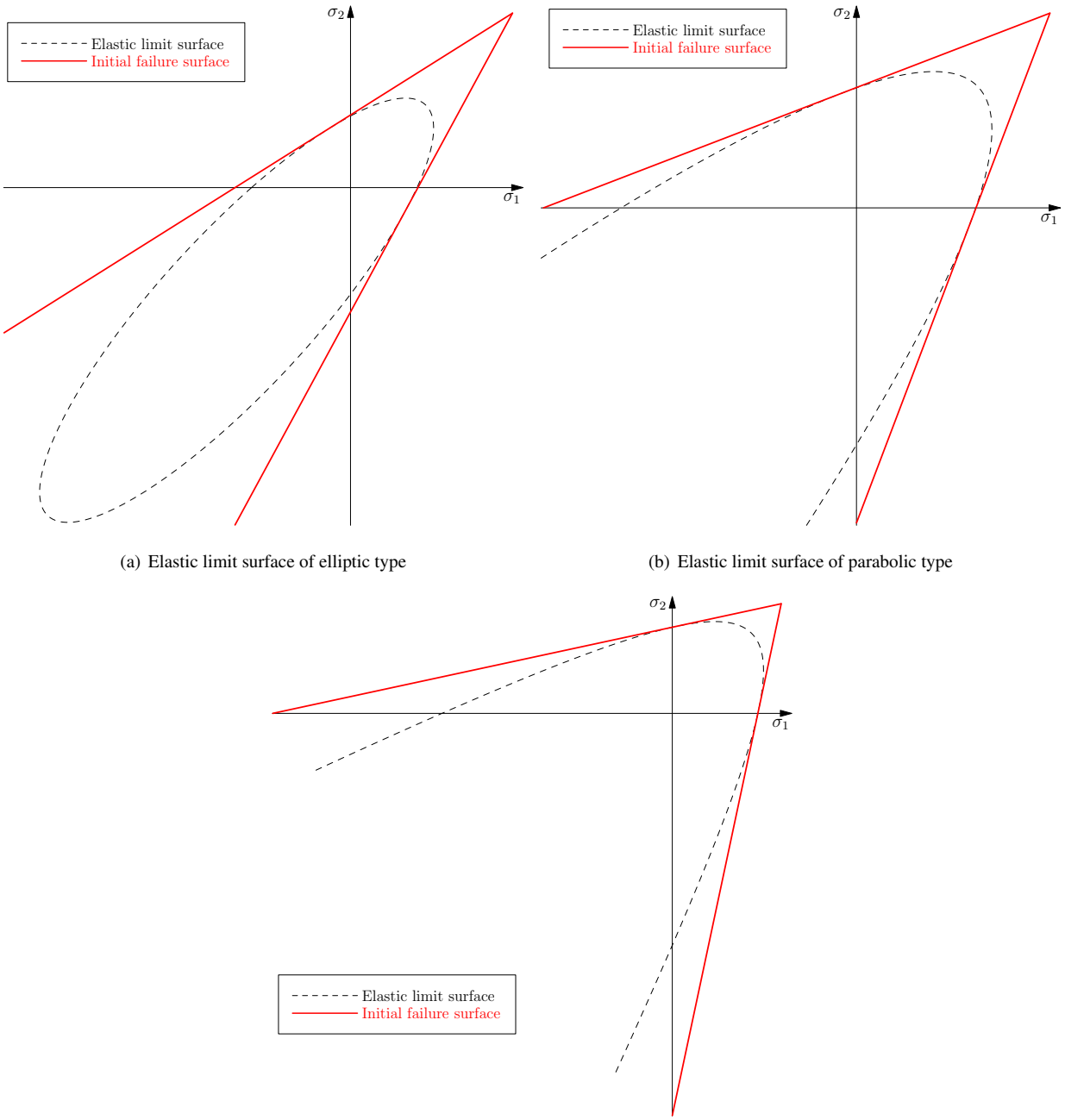

(a) Elastic limit surface of elliptic type

(b) Elastic limit surface of parabolic type

(c) Elastic limit surface of hyperbolic type

Figure 13: Elastic limit surface and initial failure surface of the Drucker-Prager criterion in the condition of plane strain